Remote Sensing of Environment 265 (2021) 112623

Contents lists available at ScienceDirect

Remote Sensing of Environment

journal homepage: www.elsevier.com/locate/rse

Impact of vegetation water content information on soil moisture retrievals in agricultural regions: An analysis based on the SMAPVEX16-MicroWEX dataset

Jasmeet Judge [a,*], Pang-Wei Liu [b,c], Alejandro Monsiváis-Huertero [d,*], Tara Bongiovanni [e], Subit Chakrabarti [f], Susan C. Steele-Dunne [g], Daniel Preston [a], Samantha Allen [a], Jaime Polo Bermejo [g], Patrick Rush [a], Roger DeRoo [h], Andreas Colliander [i], Michael Cosh [j]

[a] Center for Remote Sensing, Department of Agricultural and Biological Engineering, Institute of Food and Agricultural Sciences, University of Florida, Gainesville, FL, USA
[b] NASA's Goddard Space Flight Center, Greenbelt, MD 20771, USA
[c] Science Systems and Applications, Inc., Lanham, MD, 20706, USA
[d] Escuela Superior de Ingeniería Mecánica y Eléctrica Ticomán, Instituto Politécnico Nacional, Miguel Othon de Mendizabal S/N, Col. La escalera, Mexico City 07320, Mexico
[e] Bureau of Economic Geology, Jackson School of Geosciences, Univ. of Texas at Austin, Austin, TX, USA
[f] Indigo Ag, Inc., Boston, MA, USA
[g] Department of Geoscience and Remote Sensing, Faculty of Civil Engineering and Geosciences, Delft University of Technology, 2628, CN, Delft, the Netherlands
[h] Department of Climate and Space Sciences and Engineering, University of Michigan-Ann Arbor, Ann Arbor, MI, USA
[i] NASA Jet Propulsion Laboratory, California Institute of Technology, Pasadena, CA, USA
[j] USDA ARS Hydrology and Remote Sensing Laboratory, Beltsville, MD, USA

ARTICLE INFO

Editor: Jing M. Chen

Keywords:
SMAP
Active and passive microwave
Vegetation water content
Soil moisture
SMAPVEX16-IA
SMAPVEX16-MicroWEX

ABSTRACT

Soil moisture (SM) retrieval in agricultural regions during the growing seasons is particularly challenging due to high spatial variability and dynamic vegetation conditions. The retrievals have been problematic even when the passive signatures at different spatial scales match well since they depend upon the accuracy of vegetation information such as the vegetation water content (VWC). The VWC used in the Soil Moisture Active Passive (SMAP) single channel retrieval algorithm (SCA) is derived from remotely sensed, climatologically-based Normalized Difference Vegetation Index (NDVI), which does not respond to real-time vegetation dynamics and is prone to saturation. This study explored the differences and seasonal trend in passive signatures and SM at satellite- and field-scales and investigated uncertainties in retrievals arising from different approaches used to estimate VWC from optical and radar indices. It used high temporal resolution, ground-based data collected during the SMAP Validation-Microwave Water, Energy Balance Experiment in 2016 (SMAPVEX16-MicroWEX) during a growing season of corn and soybean. Overall, the brightness temperatures (T_B) from SMAP matched well with the upscaled, ground-based T_B, with a root mean square differences (RMSDs) of about 5 K. In contrast, the SMAP SM retrievals were worse during rapid vegetation growth in the mid-season, with higher RMSDs compared to the upscaled *in situ* SM, than those in the late-season. In addition, the ground-based T_B from corn and soybean were similar in the early and the late seasons, while their emission differences were > 40 K in the mid season. This indicates the importance of accurate VWC information, particularly during the early and late growing seasons, to account for sub-pixel heterogeneities in agricultural regions. VWC obtained from five optical and radar indices were used in the SMAP SCA for soil moisture retrieval for the entire growing season of corn. The NDVI-based VWC provided SM retrievals that were consistently lower compared to those using *in situ* VWC, with a higher RMSD of 0.030 m^3/m^3 and a negative bias of 0.020 m^3/m^3 for VWC > 4 kg/m^2. The Normalized Difference Water Index (NDWI)-derived VWC resulted in lower SM retrieval RMSD of 0.022 m^3/m^3 when compared with *in situ* SM. Among the three radar indices, vertically polarized cross-pol ratio (CR_{vv})-derived VWC provided similar RMSDs in retrieved SM as the NDWI-derived VWC during the growing season. The radar vegetation index (RVI)-derived VWC improved in the late season compared to the *in situ* VWC and resulted in SM retrievals with RMSDs

* Corresponding author.
E-mail address: jasmeet@ufl.edu (J. Judge).

https://doi.org/10.1016/j.rse.2021.112623
Received 8 March 2020; Received in revised form 16 July 2021; Accepted 24 July 2021
Available online 1 September 2021

similar to the CR_{vv}-derived retrievals. Results presented here suggest that SMAP SCA SM retrievals could be improved through the use of near-real time NDWI and CR_{vv}-derived vegetation information. Microwave data are available regardless of cloud cover, so the guaranteed availability of CR_{vv} to capture seasonal and interannual variability is advantageous.

1. Introduction

Accurate knowledge of soil moisture (SM) is crucial for various hydro-meteorological and agricultural applications. Microwave remote sensing, particularly at frequencies < 10 GHz, is highly sensitive to moisture in the upper few centimeters of the soil (near-surface SM) (McNairn and Brisco, 2004; Steele-Dunne et al., 2017). For SM studies, observations at L-band frequencies of 1.2–1.4 GHz are desirable due to larger penetration depths (Ulaby and Elachi, 1990; Liu et al., 2013, 2016a; Steele-Dunne et al., 2017). Currently, the European Space Agency (ESA) - Soil Moisture and Ocean Salinity (SMOS) and National Aeronautics and Space Administration (NASA) Soil Moisture Active Passive (SMAP) missions (Kerr et al., 2001; Entekhabi et al., 2010) provide brightness temperatures (T_B) at L-band and SM products every 2–3 days at 25 km and 36 km (or 9 km enhanced), respectively. In addition, the active space-borne L-band sensor onboard the Advanced Land Observing Satellite 2 (ALOS-2) by Japanese Aerospace eXploration Agency (Kankaku et al., 2015, 2016; Motohka et al., 2017) provides backscattering coefficients (σ^0) at spatial resolutions from 3 to 10 m, which could be used to estimate SM at high spatial resolution about every 30 days. Several upcoming satellite missions ensure the continuity of L-band observations for SM estimates for the coming decades. For example, the NASA and the Indian Space Research Organization synthetic aperture radar (SAR) (NISAR) mission will provide L- and S-band observations every 12 days starting in 2022 (Rosen et al., 2015, 2016, 2017). The ESA Copernicus Imaging Microwave Radiometer (CIMR) (Donlon, 2019) will provide passive data in several microwave bands, and Radar Observing system for Europe (ROSE-L) (Pierdicca et al., 2019) will provide active L-band observations.

Recent studies have demonstrated the agreement between passive signatures at satellite and airborne scales (McNairn et al., 2015; Colliander et al., 2015, 2019). However the retrieval of SM is complicated by the sensitivity of brightness temperature to land surface conditions such as soil temperature, surface roughness, vegetation geometry, and vegetation water content (VWC). Thus, SM retrieval from microwave observations has been particularly challenging in agricultural regions due to its high spatial variability and dynamic vegetation conditions [*e.g.*(Jackson et al., 2004; Chen et al., 2005; Yilmaz et al., 2008; Cosh et al., 2010; Monsivais-Huertero et al., 2010; Nagarajan and Judge, 2013)]. Vegetation information in SM retrieval algorithms from passive observations are obtained using different approaches. For example, in the current SMOS operational model, optical vegetation indices are used to simultaneously retrieve SM and vegetation opacity information (Wigneron et al., 2017). More recently, Li et al. (2020) has used multi-angular observations of SMOS for SM retrieval that is independent of optical indices. In the current SMAP baseline retrieval algorithm, the Single Channel Algorithm (SCA), vegetation opacity is estimated using VWC from climatology-based normalized difference vegetation index (NDVI) from MODIS (O'Neill et al., 2018). However, the climatology-based indices do not capture real-time vegetation dynamics (Zwieback et al., 2018; Fan et al., 2020) and are prone to saturation, resulting in errors in SM retrievals (*e.g.* (Konings et al., 2017)).

Among many optical indices available (Roberto et al., 2016), NDVI and normalized difference water index (NDWI) have been most widely used for estimating VWC (Jackson et al., 2004; Yilmaz et al., 2008; Cosh et al., 2010; Hunt et al., 2011; Gao et al., 2015; Cosh et al., 2019).

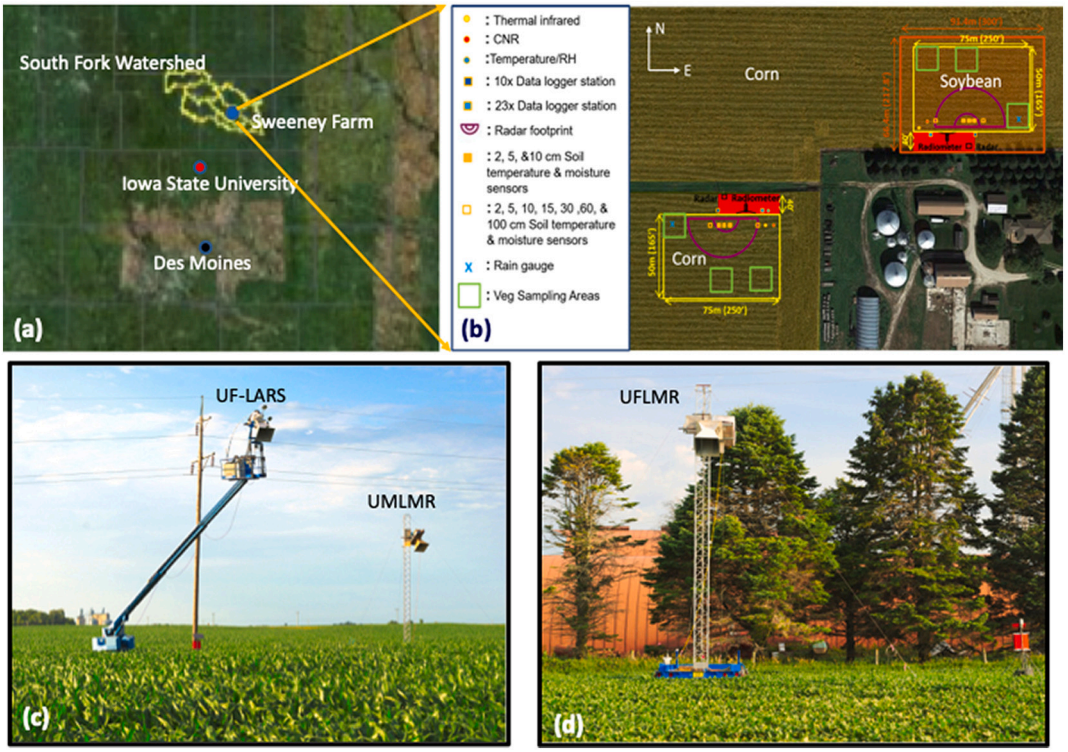

Fig. 1. (a) Location of the South Fork Watershed, Iowa; (b) Layout of sensors during SMAPVEX16-MicroWEX at the corn and soybean sites; (c) Active (UFLARS) and passive (UMLMR) microwave sensors at the corn field, and (d) Passive (UFLMR) sensor at the soybean field.

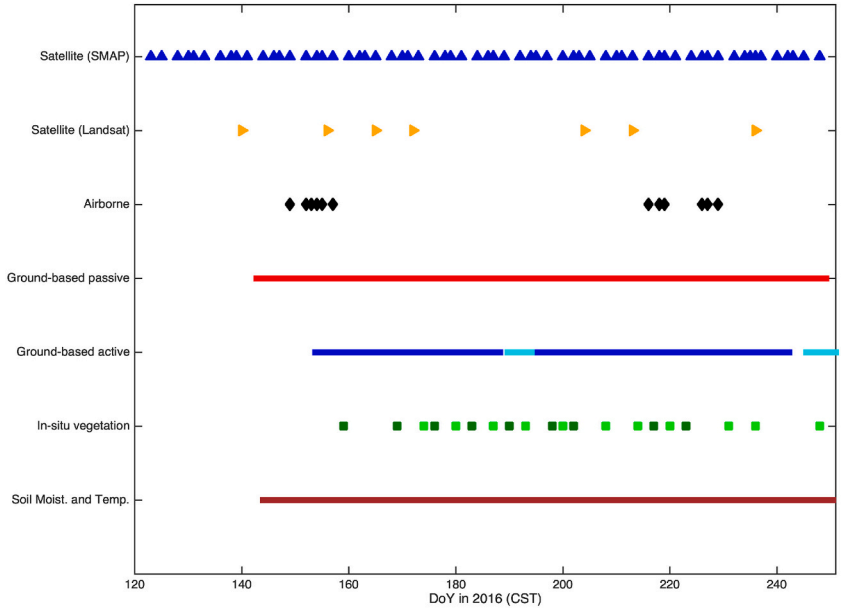

Fig. 2. Acquisition times for various observations during SMAPVEX16-MicroWEX. For ground-based active observations, the blue line represents corn and cyan line represents soybean observation dates. For *in situ* vegetation observations, dark green and light green squares represent corn and soybean sampling dates, respectively. (For interpretation of the references to colour in this figure legend, the reader is referred to the web version of this article.)

However, optical data are unavailable during cloudy conditions. In addition, though these indices may be stable under low vegetation conditions, particularly for VWC < 4 kg/m^2 (Cosh et al., 2019), they are largely insensitive to water under the canopy surface such as in stem and ears and exhibit varying degrees of saturation with increasing canopy coverage in high-biomass crops such as corn. The SMAP retrieval algorithm uses a stem factor to address this insensitivity with NDVI (Hunt et al., 2011; Chan et al., 2016). Radar-based indices such as radar vegetation index (RVI) and cross-pol ratios (CRs) have been proposed as an alternative to optical data [*e.g.* (Kim et al., 2012, 2014; Huang et al., 2015; Liu et al., 2016a; Vreugdenhil et al., 2018)]. However, RVI and CRs are affected by soil under low vegetation conditions, and are

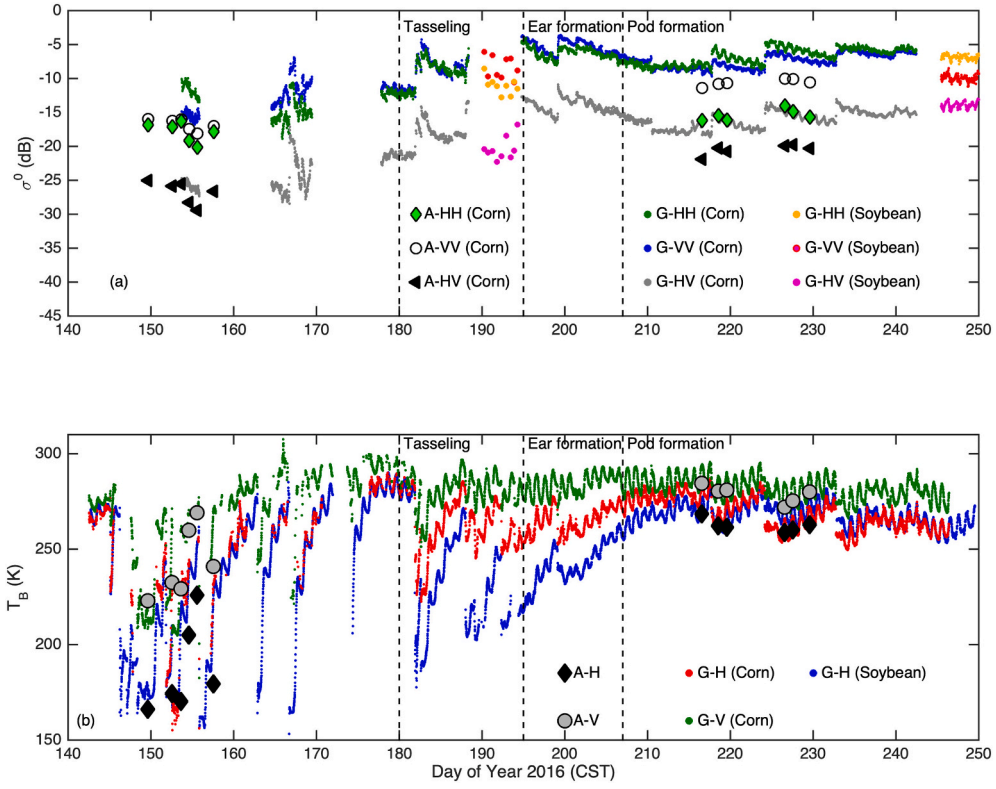

Fig. 3. Microwave observations during SMAPVEX16-MicroWEX. (a) Backscattering coefficients and (b) Brightness temperatures. 'A' represents airborne measurements from PALS and 'G' represents ground-based observations from UF and UM sensors.

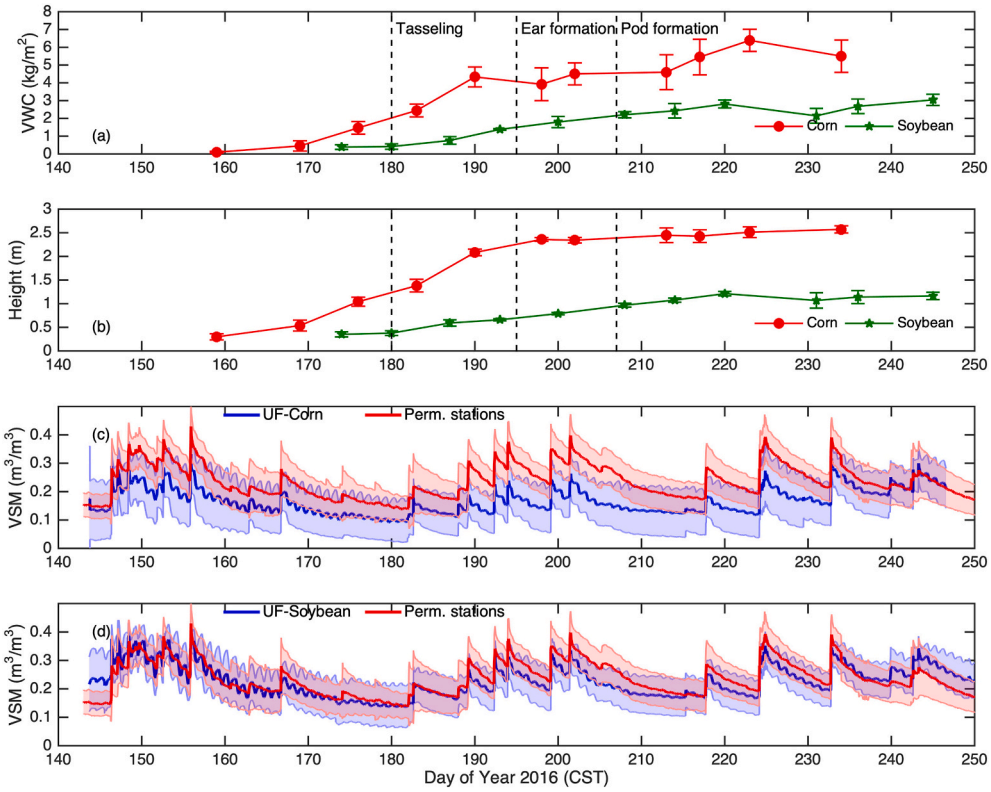

Fig. 4. *In situ* observations of (a) VWC, (b) plant height at the corn and soybean fields during SMAPVEX16-MicroWEX, (c) mean and standard deviations of 0–5 cm SM at the corn site, and (d) mean and standard deviations of 0–5 cm SM at the soybean site.

sensitive to vegetation structure and geometry, in addition to VWC, as the season progresses. A significant challenge still exists in understanding how these different approaches to estimate VWC impact SM retrievals at various phenological stages during the growing season, largely due to the scarcity of season-long concurrent active and passive (AP) microwave and optical datasets in agricultural regions.

The goal of the study is to address this challenge in SMAP SM retrievals for agricultural regions. Specifically, we investigate differences and seasonal trend in T_B and SM from satellite to field-scale during the entire growing season of corn and soybean from an intensive field experiment, Microwave Water and Energy Balance Experiment (SMAPVEX16-MicroWEX), conducted as part of the Soil Moisture Active Passive Validation Experiment in 2016 in the US Corn Belt in Iowa (SMAPVEX16-IA). In addition, we provide insights into the uncertainties in retrievals arising from VWC formulations through a field-scale study. For VWC formulations, we use radar indices from ground-based active microwave observations and satellite optical indices. These VWC values were then used in a SM retrieval algorithm based upon the SMAP SCA (O'Neill et al., 2018) to understand their impacts on retrieved SM at field-scale.

2. SMAPVEX16-MicroWEX dataset and study sites

SMAPVEX16-IA was conducted in the South Fork watershed near Ames, Iowa, (see Fig. 1(a)) to improve early season negative bias (drier retrievals) in the Level-2 SMAP soil moisture algorithm for agricultural regions (Chan et al., 2016) and erroneous sensitivity to precipitation when SMOS soil moisture was compared with *in situ* measurements (Rondinelli et al., 2015). The experiment was conducted in this rainfed, agricultural watershed (Coopersmith et al., 2015) consisting primarily of corn and soybean, for two intensive observation periods (IOP) in 2016; IOP-1, from May 28 (Day of year (DOY) 149) through June 5 (DOY 157) and IOP-2, from August 3 (DOY 216) through August 16 (DOY 229). SMAPVEX16-MicroWEX was a field-scale experiment as part of SMAPVEX16-IA and was conducted at the a commercial farm, Sweeney Farms, Alden, Iowa, (42.39 N, 93.39 W) within the same watershed. The experiment spanned 3.5 months during the whole growing season of corn and soybean, from May 23 (144) to September 2 (DOY 246). It provided field-level, season-long, concurrent AP microwave observations for further investigating SMAP retrieval algorithms. In addition, *in situ* soil and vegetation conditions were measured at the two 3750 m^2 fields. Fig. 1(b) shows the sensor layouts for the two fields and Figs. 1(c) and (d) show the ground-based microwave sensors. Crop classification at 30 m resolution covering the SMAP pixel in the South Fork watershed was obtained from the US Department of Agriculture (USDA) Crop Data Layer (CDL)(USDA, 2016). The soil texture in the fields is silt loam with 29% clay, 11% sand, and 60% silt, based upon the USDA Soil Survey. Fig. 2 shows the time line of remote sensing and *in situ* observations during SMAPEVEX16-MicroWEX.

2.1. Microwave and optical observations

Ground-based σ^0 observations at quad-polarization were obtained at 1.26 GHz every 30–60 min using the University of Florida L-band automated radar system (UFLARS) (Nagarajan et al., 2014; Liu et al., 2016b) mounted on a genie-lift (see Fig. 3 (a)). The system was located at the corn site for the whole growing season providing 3300 observations, except for two 1-week periods, DOY 189–194 and DOY 245–250, during which it monitored backscatter at the soybean site, providing 523 observations (see Fig. 2). Weekly calibrations were conducted using a single-target calibration technique with a trihedral corner-reflector. Mean amplitude of backscatter was obtained by averaging independent samples spatially, from −9 to +9 azimuth and spectrally, from 1130 to 1370 MHz to reduce the standard deviation of fading (Hoekman, 1991; Liu et al., 2016a, 2016b; Vermunt et al., 2020). The overall uncertainty of UFLARS measurements is 1.71 dB (Liu et al., 2016b).

Over 8000 V- and H-pol ground-based T_B observations for corn were obtained using a dual-channel L-band radiometer from the University of Michigan (UMLMR) and similar number of H-pol observations for soybean were obtained from the single channel L-band radiometer from the University of Florida (UFLMR) (see Fig. 3(b)). Both the radiometer systems, built by the University of Michigan, share the same design and operate at the central frequency of 1.41 GHz. Microwave emissions from growing corn and soybean footprints of about 50 m^2 were observed every 15 min at an incidence angle of 40. The radiometers were calibrated weekly using the internal calibration technique (Tien et al., 2007). The overall uncertainty of measurements were 2 K (Tien et al., 2007; Liu et al., 2016a).

In addition to the ground-based microwave data, twelve airborne AP L-band observations at a spatial resolution of 600 m were obtained concurrent with the SMAP overpasses during IOP-1 and IOP-2 from the Passive Active L-band System (PALS) (Colliander et al., 2019), as shown in Fig. 2. Satellite observations include 109 dual-pol observations of SMAP L1CTB (v.6,R16010–001) at 36 km with an incidence angle of 40 and corresponding retrieved SM products from SMAP L2 SM P (v.6, R16010–001) at 36 km were obtained during SMAPVEX16-MicroWEX. Satellite-based optical indices, NDVI and NDWI, were obtained at 30 m from Landsat 8 products, LC8NDVI and LC8NDMI, respectively, for the corn site. The indices from four Landsat pixels covering the corn site were averaged to represent overall vegetation condition at the site. In this study, we compare these multiscale observations using root mean square differences (RMSDs) and unbiased RMSDs (ubRMSD) defined in the eq. 1 below.

$$\mathrm{RMSD} = \sqrt{\frac{1}{n}\Sigma_{i=1}^{n}(x_i - y_i)^2}; \qquad \mathrm{ubRMSD} = \sqrt{\mathrm{RMSD}^2 - \mathrm{bias}^2} \tag{1}$$

where x_i and y_i represent the corresponding values of the two datasets, and n represents the total number of points.

2.2. Vegetation and soil observations

Corn of cultivar Pioneer 1365 and ecotype IB001 was planted on DOY 125 and soybean of cultivar Pfizer 20R23 and ecotype SB0301 was planted on DOY 128. Both crops were planted at a row spacing of 0.76 m. Weekly vegetation observations were conducted for plant density, phenology, structure, geometry, leaf area index (LAI), biomass by components, and vegetation water content (VWC) from three sampling areas, shown in Fig. 1(b). The average plant density for corn was 13 plants/m^2 and that of soybean was 24 plants/m^2 during the growing season. To obtain structure, geometry, and wet above ground biomass of leaves, stems and ears/pods, four plants were sampled at random in each of the three vegetation sampling areas. The plants were dried at 48°C for 3–7 days, depending upon the amount of vegetation material, to obtain dry biomass of the components. The sampling protocols were the same as those used in our previous MicroWEXs conducted in Florida and are detailed in (Yang et al., 2005; Casanova et al., 2006; Bongiovanni et al., 2015a, 2015b). Figs. 4(a) and (b) show the *in situ* VWC and plant heights along with the phenological stages, respectively.

In situ SM and soil temperatures were observed at three locations (see Fig. 1(b)) in both corn and soybean fields every 15 min using time domain reflectometry (TDR) probes (CS-616 from Campbell Scientific) and thermistors, respectively, at depths of 2, 5, 10, 15, 30, 60, and 120 cm. Three TDRs were installed at 2 and 5 cm for each station to provide a better estimate of variability in the near surface. The probes were calibrated using gravimetric measurements during a two week period, following established protocols, *e.g.* (Bhuiyan et al., 2018). The calibration error was 0.02 m^3/m^3, which was 0.05 m^3/m^3 lower than that obtained using the manufacturer's calibration coefficients. In this study, the SM values observed close to the radiometer and radar footprints were averaged to obtain SM at 0–5 cm. Figs. 4 (c) and (d) show the mean and the standard deviations (SD) (defined as $\sqrt{\frac{1}{n}\Sigma_{i=1}^{n}(x_i - \overline{x})^2}$, where x_i and $\overline{x}$ represent the i^{th} value and the mean of the dataset, respectively, and n represents the total number of points in the dataset) of the near-surface SM in the top 5 cm at the corn and the soybean sites, respectively. In these figures, the *in situ* SM at the two field sites are also compared with the mean and the SD of the SM from 20 permanent *in situ* network stations that were operated by the USDA-Agricultural Research Service, located within the SMAP pixel (Colliander et al., 2019). The SM within the SMAP pixel was very heterogeneous with differences at 5 cm of up to 20% by volume. The near-surface SM observed at the corn and the soybean sites during SMAPVEX16-MicroWEX were within the variability of the SM observed by the permanent stations, indicating their representativeness of SM conditions within the SMAP pixel.

3. Methodology

3.1. SM retrieval algorithm

To gain insights into the impact of VWC estimates on SM retrieval, field-scale *in situ* observations were used in this study to avoid scaling errors inherent with satellite-scale analyses. The SM retrieval was conducted only for the corn site using ground-based T_B observations since the soybean field site was surrounded by corn fields and the NDVI and NDWI products may be contaminated due to mixed-pixels.[1] The emission model for SM retrieval followed the SCA algorithm for SMAP passive retrievals (O'Neill et al., 2018) with the primary equation as:

$$T_{Bp} = T_s e_p exp\left(-\tau_p sec\theta\right) + T_c\left(1-\omega_p\right)\left[1-exp\left(-\tau_p sec\theta\right)\right]\left[1+r_p exp\left(-\tau_p sec\theta\right)\right] \tag{2}$$

where the subscript p is H or V polarization, e_p is the soil emissivity = 1 - r_p, T_s and T_c are the soil and vegetation temperatures, τ_p is the nadir vegetation opacity, ω_p is the vegetation single scattering albedo, and r_p is the rough soil reflectivity. Typically, ω_p is assumed zero at L-band, and $T_s = T_c$ = effective temperature, T_{eff}, which is estimated as (O'Neill et al., 2018):

$$T_{eff} = K[T_{soil2} + C(T_{soil1} - T_{soil2})] \tag{3}$$

where T_{soil1} and T_{soil2} are the soil temperatures at 0–10 cm and 10–20 cm soil layers, respectively, K is a constant = 1.007 for agricultural terrain and C = 0.246 for morning and = 1 for afternoon acquisitions. In this study, the T_{soil1} and T_{soil2} were obtained from *in situ* observations.

The r_p is estimated as a function of specular refelectivity, r_{0p}, and three empirical parameters, Q, related to polarization-mixing, and h and n, related to soil roughness (Wang and Choudhury, 1981; Wigneron et al., 2017):

$$r_p = \left[(1-Q)r_{0p} + Qr_{0q}\right]e^{h_p cos^{n_p}(\theta)} \tag{4}$$

For this study, soil dielectric constant, ϵ, for estimating specular reflectivity was obtained using mineralogically-based model from Liu et al. (2013) and Mironov et al. (2009) and Q = 0.35 (Mialon et al., 2012; Lawrenmce et al., 2013). The parameters h and n were obtained through optimization with respect to ground-based observations of T_{Bv} (for h_v and n_v) and T_{Bh} (for h_h and n_h), using *in situ* SM. The optimization was conducted during the early season, in the first 40 days after planting (DOY 125–165), when LAI < 0.3 and plant height < 20 cm. The convergence was reached when the difference between the estimated T_B and ground-based T_B was ≤ 0.4 K, corresponding to the precision of ground-based observations.

The τ_p is a linear function of VWC scaled by an empirical parameter, b, that is dependent on many factors such as vegetation type, polarization (Van de and Wigneron, 2004; O'Neill et al., 2014), and phenology

[1] Originally, the farmer had planned to plant only corn at Sweeney Farms. However, a 3750 m^2 field was dedicated to soybean to allow concurrent ground-based observations during SMAPVEX16-MicroWEX.

(Dugwon et al., 2010). For this study, the b parameters at H- (b_h) and V-pol (b_v) were obtained through optimization of τ_H and τ_V with respect to T_{Bh} and T_{Bv}, respectively. The optimization was conducted during the mid and late seasons, from DOY 180 onward, when LAI >3.3 and used *in situ* observations of SM and VWC. The *in situ* VWC were interpolated to obtain a continuous time series. The convergence criterion for the estimated T_B at both polarizations was the same as that for h and n parameters described above. The optimized τ_H and τ_V were fitted to a 2^{nd} degree polynomial function, resulting in smooth time series of b_h and b_v parameters.

The SM retrieval was conducted for corn starting from DOY 180, with the optimized h, n, and b parameters using T_{Bh} and T_{Bv}, resulting in SM_h and SM_v, respectively. Retrieval scenarios with six sources of VWC included, *in situ* VWC and VWC obtained from NDVI, NDWI, RVI, and hh- and vv-pol cross-polarization ratios (CR_{hh} and CR_{vv}, respectively). Comparisons of SM_h and SM_v retrieved in these six scenarios provided insights into the impact of different VWC formulations on retrievals at different phenological stages during the corn growing season.

3.2. VWC from optical and radar indices

In this study, five indices from remotely sensed observations for VWC estimates were explored. The two optical indices, NDVI and NDWI, were obtained from Landsat, as described in section 2.1, and the three radar indices (see eq. 5), RVI (Huang et al., 2015), CR_{vv}, and CR_{hh} (Prakash et al., 2012; Vreugdenhil et al., 2018), were obtained from the ground-based observations from UFLARS during SMAPVEX16-MicroWEX.

$$\mathrm{RVI} = \frac{8\sigma^0{}_{hv}}{\sigma^0{}_{hh} + \sigma^0{}_{vv} + 2\sigma^0{}_{hv}}; \qquad \mathrm{CR_{vv}} = \sigma^0{}_{vh} \Big/ \sigma^0{}_{vv}; \qquad \mathrm{CR_{hh}} = \sigma^0{}_{vh} \Big/ \sigma^0{}_{hh} \tag{5}$$

As in the SMAP retrieval algorithm, the VWC from Landsat NDVI in this study was estimated using eq. (19) in (O'Neill et al., 2018) as below:

$$\mathrm{VWC} = 1.9134\ \mathrm{NDVI}^2 - 0.3215\ \mathrm{NDVI} + \text{stem factor}\ \frac{\mathrm{NDVI}_{max} - \mathrm{NDVI}_{min}}{1 - \mathrm{NDVI}_{min}} \tag{6}$$

where, $NDVI_{max}$ and $NDVI_{min}$ are the annual maximum and minimum NDVI values for the location, respectively. In the SMAP algorithm, the $NDVI_{max}$ for croplands is set to the observed NDVI (O'Neill et al., 2018), the same as the NDVI in the first two terms. In this study, the NDVI (and hence, $NDVI_{max}$), was obtained from Landsat. The default value for the $NDVI_{min}$ in the SMAP algorithm for croplands is 0.1 (O'Neill et al., 2018). In our field-scale implementation of the SMAP algorithm with best available data, the $NDVI_{min}$ was set to 0.24, which was the minimum value observed during the SMAVPEX16-MicroWEX season, on DOY 140. The stem factor is the maximum amount of water in the stems and is 3.5 for crops in the SMAP algorithm (O'Neill et al., 2018). In this study, we found that the stem factor of 3.9 provided the best regression of *in situ* VWC with Landsat NDVI.

The VWC from NDWI was estimated using regression of Landsat NDWI and *in situ* VWC. This NDWI-derived VWC was also compared with that obtained using the regression equation by (Cosh et al., 2019):

$$\mathrm{VWC} = 10.184{*}\mathrm{NDWI} + 1.0026 \tag{7}$$

In (Cosh et al., 2019), the above coefficients were obtained using VWC observations from four days during IOP-1 and IOP-2 for 5 corn fields in the SMAP pixel during SMAPVEX16-IA, while in this study the coefficients were obtained using observations from the whole SMAPVEX16-MicroWEX season. The VWC from the two radar indices, RVI and CR, were estimated using regression with the *in situ* VWC.

4. Results and discussion

4.1. Microwave observations during SMAPVEX16-MicroWEX

Fig. 3(a) shows the ground and airborne active microwave observations. The ground-based active observations for corn match well with the airborne data at VV and cross-pol, with mean differences of 2.5 dB during IOP-1 and 3 dB during IOP-2. However, the differences were higher at HH-pol, with PALS observations lower than the ground-based values by about 8 dB. The ground-based HH and VV observations in corn converge around tasseling (around DOY 180), with increasing contribution of direct vegetation scattering, and the cross-pol backscatter was consistently 8–9 dB lower than co-pol observations, similar to the behavior observed during our previous experiments with sweet corn in Florida (Liu et al., 2016a). Diurnal variations, particularly during non-rainy periods, were observed during a fully-grown corn canopy, with morning backscatter at 6 a.m. local time, about 0.45 dB higher than that in the evening, at 6 p.m., with larger differences at HH than VV. This phenomenon has also been studied in detail by prior studies (Steele-Dunne et al., 2012; Konings et al., 2017; van Emmerik et al., 2017; Vermunt et al., 2020). Vermunt et al. (2020) conducted an extensive ground validation with destructive sampling and sap flow measurements to show that the subdaily variations in VWC are significant. Some of the variations, particularly backscatter maxima around sunrise were attributed to dew accumulation. Diurnal cycles in backscatter were also observed for soybean in the late season, similar to those in corn.

In the early season, the average sensitivity of corn backscatter to SM is 0.5 dB/%vol of SM, primarily corresponding to rainfall events. However, in mid and late season, the sensitivity of the backscatter decreases to 0.25 dB/%vol. Even though the corn canopy was fully mature, after DOY 210, the sensitivity is still considerable, as seen in Figs. 3(b) and 4(c), since the backscatter is increasingly dominated by double scattering that accounts for the soil-vegetation interactions (Monsivais-Huertero et al., 2018; Monsivais-Huertero et al., 2010). This phenomenon observed from field measurements confirms findings from previous studies using forward modeling to investigate scattering mechanisms of backscatter in vegetated surfaces (Tavakoli et al., 1991; Stiles et al., 2000; Monsivais-Huertero and Judge, 2011; Monsivais-Huertero et al., 2018; Sharma et al., 2020). In addition, the HH and cross-pols were found to be the most sensitive to SM during rain events, with changes of about 3 dB.

For soybean, the average σ^0 values were − 8.7, −9.13, and − 17.23 dB at HH, VV, and HV pols, with HH > VV in late season, similar to those observed by (Kim et al., 2012). However, the differences between cross- and co-pol values were about 8 dB during SMAPVEX16-MicroWEX, which were lower than those reported in (Kim et al., 2012). The observations during a week in the mid season show rapid changes in response to frequent precipitation (see Fig. 4(d)), compared to those during the late season.

Figs. 3(b) show the ground-based and airborne passive microwave observations. As expected, H-pol T_B for corn and soybean are similar during the early season, as shown in Fig. 6, as both are largely determined by the soil moisture and soil properties. Around DOY 180, corn reaches the tasseling stage and its VWC exceeds 2 kg/m^2 (see Fig. 4(a)), so the T_B becomes increasingly influenced by the vegetation rather than the soil (Ulaby et al., 2014). Meanwhile, the *in situ* VWC in soybean is still much lower, and the T_B of the soybean is still primarily influenced by the soil. The two converge again around DOY 210, when the soybean reaches maximum biomass of 2 kg/m^2, pods start to form, and the sensitivity to soil moisture in both fields is similar. The divergence in T_Bs by > 50 K between the two crop types between DOY 180 and DOY 210

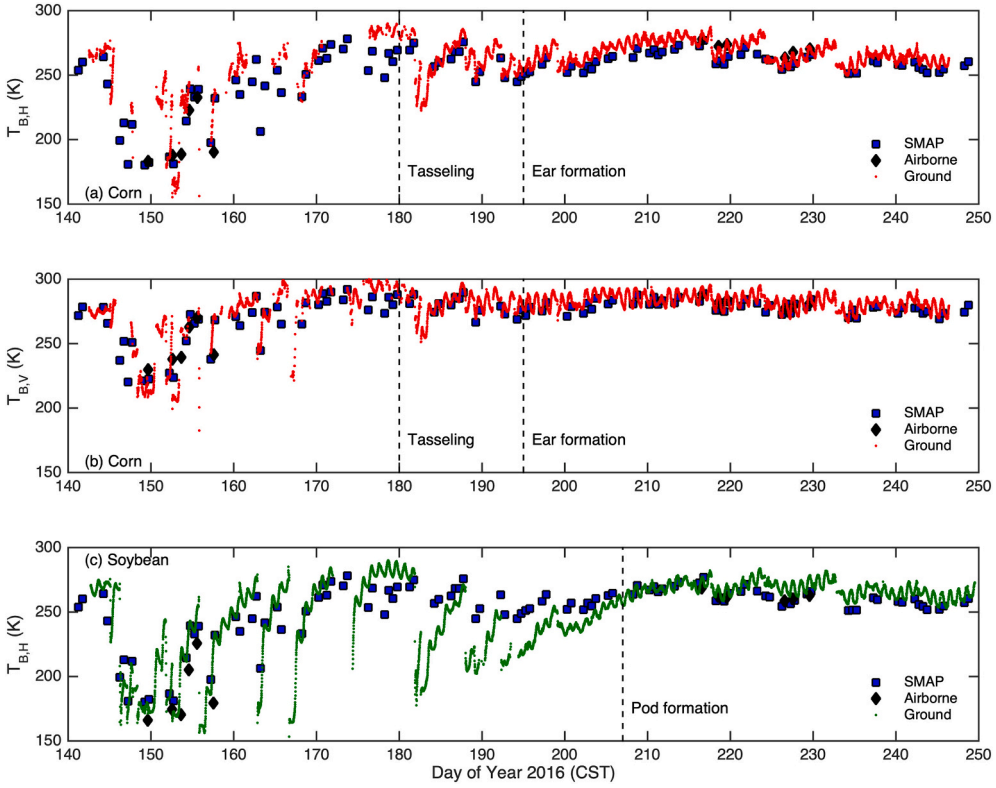

Fig. 5. Comparison of T_B from satellite (SMAP - 36 km), airborne (PALS - 600 m), and ground-based for corn and soybean fields.

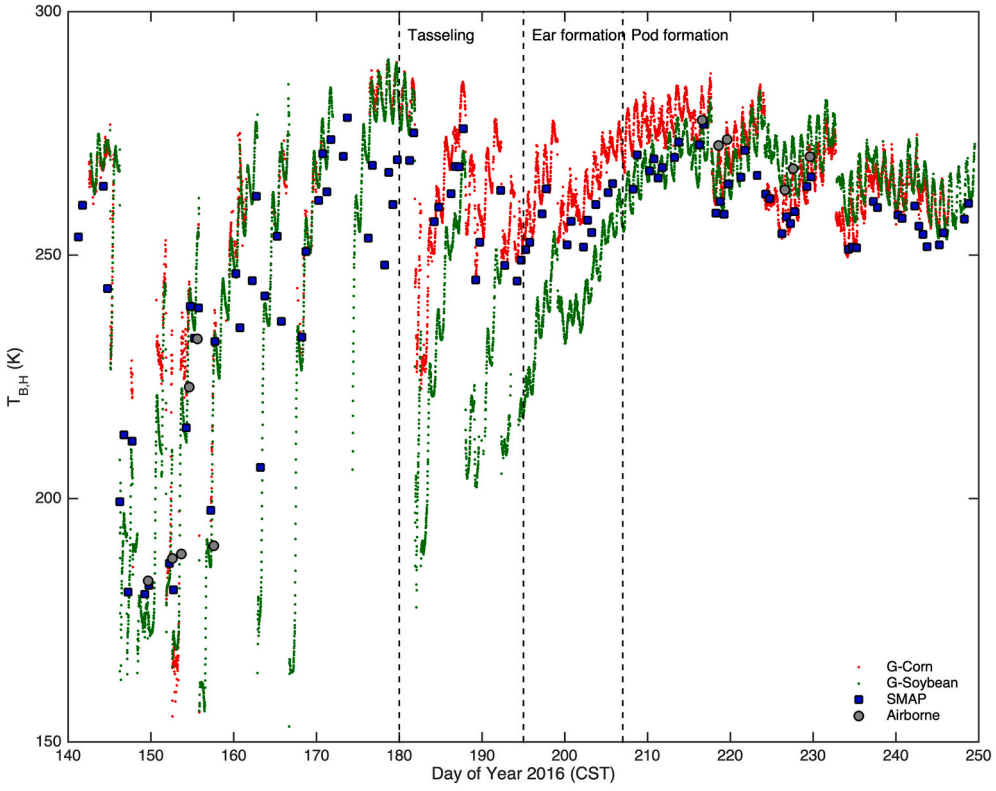

Fig. 6. H-pol TB from SMAP, PALS, UMLMR, and UFLMR for corn and soybean fields. The satellite observations from SMAP are generally enveloped by ground-based corn and soybean signatures from UMLMR and UFLMR, respectively. 'G' represents ground-based measurements from UF and UM sensors.

Table 1
Comparison of H-pol T_B observed from SMAP, PALS, and ground-based radiometers at their native resolutions. RMSD and ubRMSD are also presented for the SMAP and the upscaled ground-based T_B at 36 km.

Overall	RMSD (K)	ubRMSD (K)
SMAP & Corn site	6.67	6.28
SMAP & Soybean site	14.14	14.14
SMAP & Site-upscaled	5.90	5.08
SMAP & PALS (IOP1 & IOP2)	14.94	14.85
PALS & Corn site (IOP1 & IOP2)	24.72	22.31
PALS & Site-upscaled (IOP1 & IOP2)	23.73	16.72

Mean Air Temperature
291.26 K

underscores the need to account for sub-footprint spatial heterogeneity in agricultural areas. It is particularly important as this divergence occurs in a period between tasseling and ear formation for corn, during which soil moisture availability has a significant impact on yield (Claassen and Shaw, 1970; Denmead and Shaw, 1960) and soil moisture information is essential at this time.

Overall, the differences between the ground-based T_B at the two polarizations in corn were higher in the early season, with a mean difference of 23 K. As the corn grew and emission was increasingly dominated by the vegetation, the differences decreased to 3 K when VWC was > 4.5 kg/m^2 and the corn height was 2.5 m, as shown in Figs. 4(a and b). In both corn and soybean, the sensitivities of T_B to SM was higher during

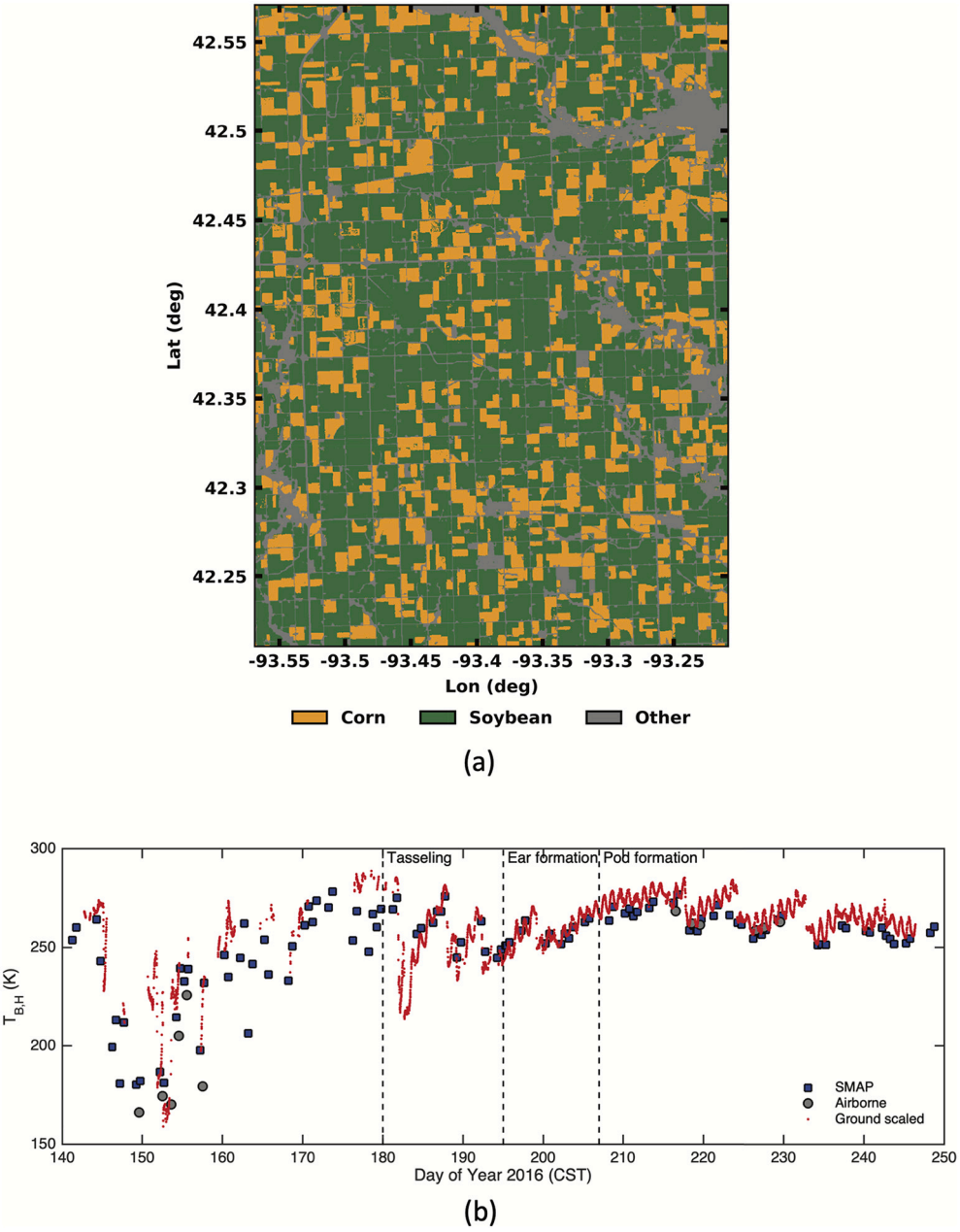

Fig. 7. (a) Land cover fraction in the 36 km SMAP pixel from the US Department of Agriculture (USDA) Crop Data Layer (CDL) (USDA, 2016) and (b) Upscaled ground-based H-pol TB compared with the SMAP and the PALS observations at 36 km.

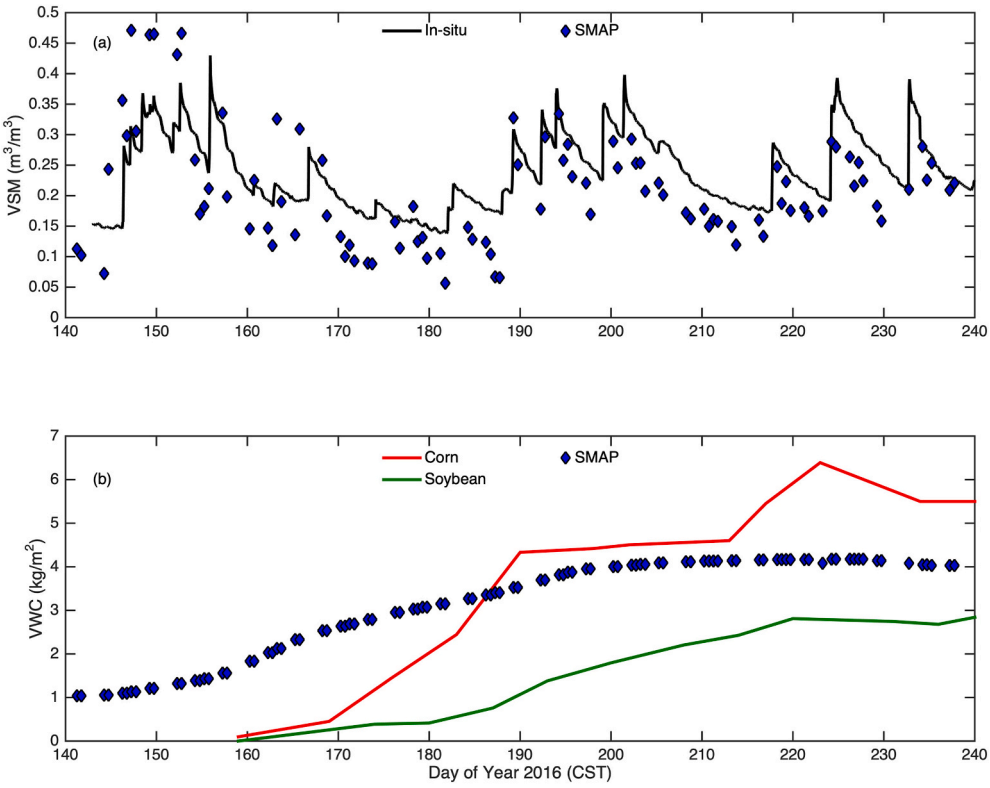

Fig. 8. (a) Upscaled *in situ* SM from 20 permanent stations in the SMAP pixel compared with the retrieved SM from SMAP at 36 km. (b) VWC estimated in the SMAP retrieval algorithm at 36 km compared to the *in situ* VWC at the corn and soybean sites during SMAPVEX16-MicroWEX.

early season with an average of 5.25 and 4.33 K/% vol at H-pol, respectively. In the late season, the average sensitivities decreased to 1.54 and 0.69 K/%vol for corn and soybean, respectively. The sensitivities at H-pol in corn were higher than V-pol which were 1.6 and 0.7 K/%vol during the early and late seasons, respectively.

The PALS airborne observations at 600 m encompassed the corn field and the footprint of the ground-based radiometer at the corn site. Both the airborne and the ground-based T_Bs showed similar responses to SM changes during IOP-1 and IOP-2 (Fig. 3(b)). Overall, the PALS T_B were lower than ground-based at both pols, with a bias of around 6–7 K. The differences in the early season (IOP-1) were higher at around 25–30 K, largely due to scene heterogeneities within the PALS footprint compared to the field-site from variable soil moisture conditions (see Fig. 4(c)). The differences reduced to 3–5 K as the scene became increasingly homogeneous with mature vegetation.

Figs. 5(a, b, and c) show the time series of the satellite, airborne, and ground-based T_B observations at their native spatial resolutions, and Fig. 6 provides a close-up of the comparison at H-pol. Even with large differences in their spatial scales, the SMAP and ground-based observations matched well and captured dynamic moisture conditions during the growing season. Table 1 shows the RMSDs and ubRMSDs between the T_{Bh} from SMAP, PALS, and from the ground-based radiometers at the corn and soybean sites. The RMSDs and ubRMSDs between SMAP and the corn site T_{Bh} were lower than those between SMAP and the soybean site, due to a higher fraction of corn and spatial variability in soil moisture within the satellite footprint. This can also be seen in Fig. 6 where, as the season progressed, the SMAP T_{Bh} were between ground-based T_{Bh} observations from corn and soybean, with values closer to corn than soybean. Overall, the RMSDs and ubRMSDs of T_B between PALS and SMAP were about 15 K, similar to the high differences between PALS and the ground-based observations. Since, PALS acquisition was limited to two IOPs, the sample size of 12 observations was limited.

We used CDL at 30 m (Fig. 7 (a)) to upscale ground-based T_B observations based upon fractions of corn and soybean pixels at the SMAP and PALS scales. The SMAP pixel consisted of 60% corn and 23% soybean, and the PALS pixel consisted of 72% corn and 10% soybean. The ground based T_{Bh} signatures from corn and soybean were combined, with weights based upon their land cover fractions using linear spectral mixing (Clevers and Zurita-Milla, 2008) to obtain effective, upscaled T_{Bh} for the mixed satellite and airborne pixels. The differences between the upscaled T_B and the satellite/airborne pixels were reduced (see Table 1). For example, the RMSD and ubRMSD between SMAP and the upscaled-ground based T_B were reduced to 5.9 and 5 K, respectively, indicating that the corn and soybean signatures at the SMAPVEX16-MicroWEX sites were representative of those in the region (see Fig. 7b and Table 1).

4.2. SM observations during SMAPVEX16-MicroWEX

Even though the upscaled ground and satellite T_{Bh} observations in Fig. 7 (b) matched well throughout the season, the retrieved SM from SMAP shows significant differences from the upscaled SM, as shown in Fig. 8 (a). The upscaled SM was obtained from 20 permanent SM stations, using the SMAP default approach with the Voronoi diagram technique that partitions a plane into Thiessen Polygons (Dingman, 2015) based upon the distance of a group of points to each other within the polygon (Colliander et al., 2017b; Bhuiyan et al., 2018; Colliander et al., 2019). The RMSD and bias between SMAP-derived and the upscaled SM during the growing season were 0.064 and − 0.024 m^3/m^3, respectively. These differences are similar to those found by (Colliander et al., 2017b,a; Walker et al., 2019). The RMSD and bias during the nearly-bare conditions, within 20 days of planting at the field site, was 0.1 and 0.03 m^3/m^3, respectively. Since the emission during this time is primarily controlled by soil properties, the heterogeneity in the SMAP pixel could result in these differences. The RMSD and bias decreased during the early vegetative period prior to tasseling, such as DOY 170–180, at 0.05 and − 0.05 m^3/m^3, respectively, when both corn and soybean VWC < 2 kg/m^2 (Fig. 4(a)) and their T_B values were still similar (Fig. 6). After this period, the emission transitions from soil to

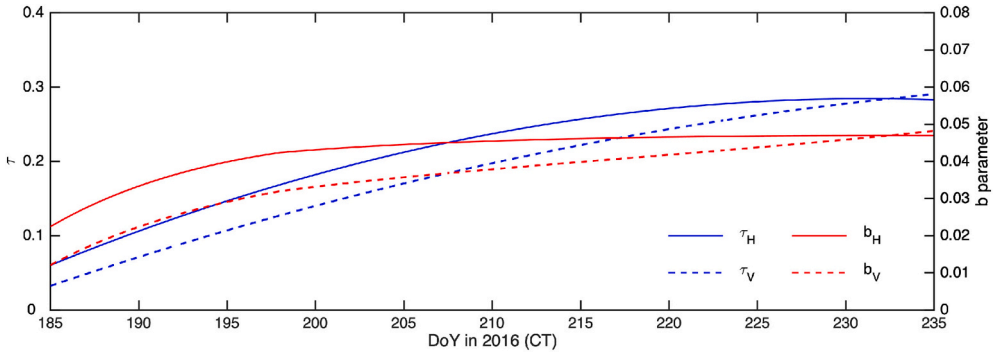

Fig. 9. Optimized vertical and horizontally polarized vegetation opacities, τ_H and τ_V, respectively, obtained from the microwave emission model at the corn site during SMAPVEX16-MicroWEX.

Table 2
Retrieval equations for VWC using optical and microwave indices in corn. The metrics, Pearson correlation coefficient (R), RMSD, and bias and *P*-values, are given with respect to *in situ* VWC. The RMSDs and biases are in kg/m^2. The NDWI relationships are obtained for before and after ear formation (see Fig. 4(a)).

Index	Validity	Regression Equations	R	RMSD	Bias	p-value
NDVI	growing season	Eq. 6	0.89	1.09	0.25	1.35E-06
	growing season	$VWC = 1.50NDWI^2+8.85NDWI + 0.90$	0.97	0.52	0.05	1.04E-07
NDWI	$VWC_{total} \leq 4$ (kg/m^2)	$VWC = 16.21NDWI^2+6.99NDWI + 0.67$	0.98	0.21	0.16	7.79E-08
	$VWC_{total} > 4$ (kg/m^2)	$VWC = 2.50NDWI^2+8.41NDWI + 0.85$	0.77	0.73	0.17	0.07
RVI	growing season w/ θ=50	$VWC = -110.53RVI^2-50.03RVI + 5.35$	0.94	0.76	−0.18	0.002
CR_{vv}	growing season w/ θ=50	$VWC = -311.57CR_{vv}^2-15.16CR_{vv}-0.04$	0.98	0.47	−0.004	2.62E-07
CR_{hh}	growing season w/ θ=50	$VWC = -63.41CR_{hh}^2+47.48CR_{hh}-1.46$	0.67	1.76	−0.40	0.16

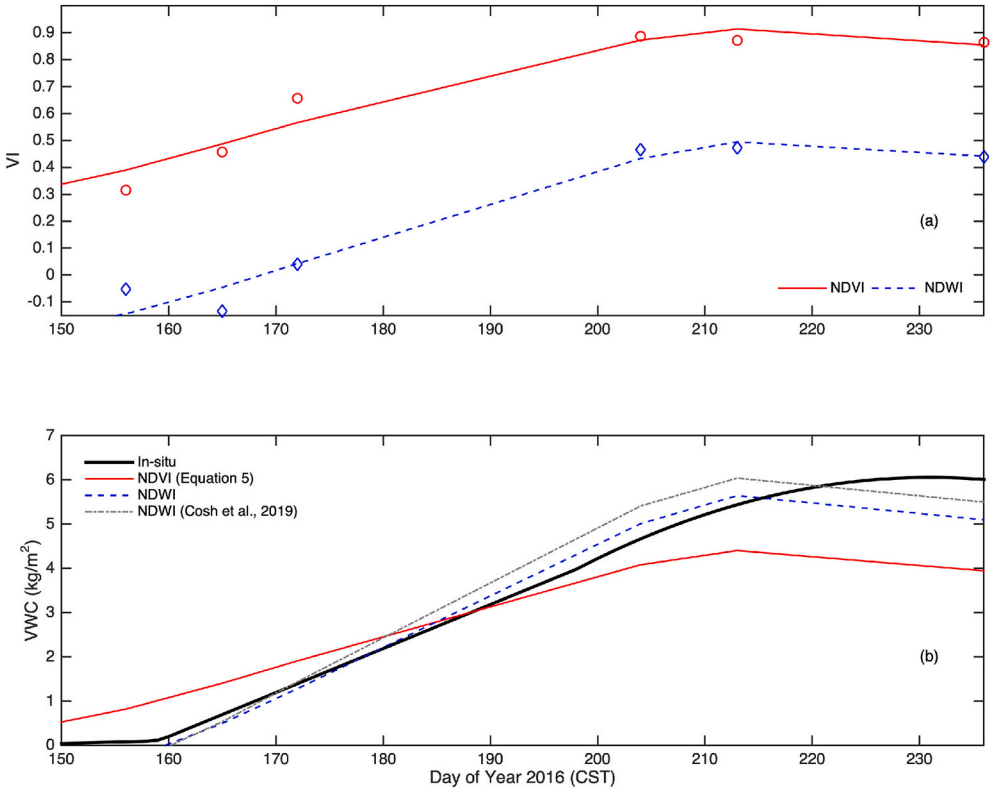

Fig. 10. Comparisons of (a) optical indices, with red circles and blue diamonds showing the indices on the dates of Landsat acquisitions, and (b) VWC estimated from NDVI using Eq. 6; from NDWI using the regression equation for the growing season in Table 2 and from NDWI using (Cosh et al., 2019) at the corn site during SMAPVEX16-MicroWEX. (For interpretation of the references to colour in this figure legend, the reader is referred to the web version of this article.)

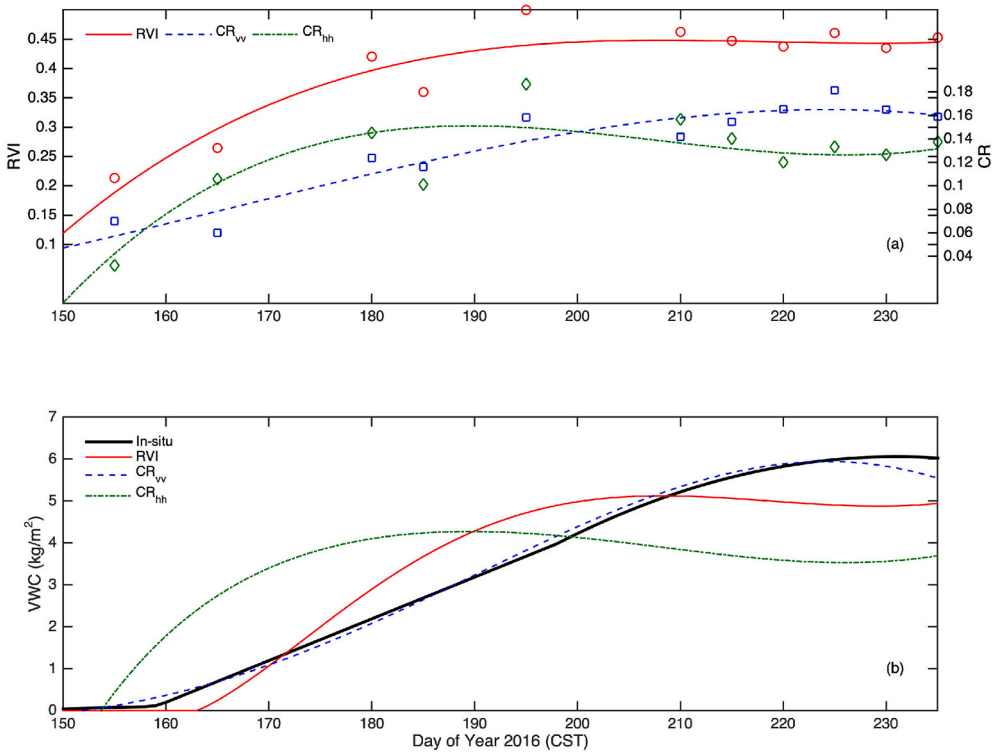

Fig. 11. Comparisons of (a) radar indices and (b) VWC estimated from RVI, CR_{vv} and CR_{hh} using the regression equations in Table 2, at the corn site during SMAPVEX16-MicroWEX.

increasingly dominated by vegetation. Hence, in the late season (*e.g.* DOY 225–235) when the plant height was maximum, the RMSD and the bias increased to 0.07 and − 0.06 m^3/m^3, respectively.

Fig. 8 (b) compares the NDVI-derived VWC at 36 km used by SMAP with *in situ* VWC at the corn and soybean sites. The SMAP VWC is non-zero before any corn or soybean were planted in the region, possibly due to other vegetation such as alfalfa. However, both the SMAP and the field-scale VWC show an increase starting around DOY 160. The SMAP VWC is mostly bounded by the corn and the soybean VWC after DOY 185, with values closer to corn during most of the season, confirming with the CDL that corn was the most dominant crop in the study region. As vegetation starts playing an important role in the retrieval algorithm, the uncertainty in VWC estimates may account for much of the difference between the SMAP and field-scale VWC. This is particularly true in agricultural regions during the growing season, when the VWC varies considerably between crops and can result in a very different brightness temperature.

4.3. Model parameters

As mentioned in Section 3.1, optimization was conducted in the early season to obtain the parameters for surface roughness components, h and n, to minimize the impacts from these parameters in the retrieval algorithm. The optimized values for the empirical parameters h_h and h_v in the roughness model were 0.1 and 0.9, respectively, characterized as a medium-rough field by Choudhury et al. (1979). These values were close to the range of 0.1–0.8 for agricultural crops as reported by Wigneron et al. (2017). The values for n_h and n_v were 1 and 0 respectively, where typical values range from −1 to 2 (Wigneron et al., 2017). The optimized values for h and n were used in the SM retrieval algorithm during the growing season.

Fig. 9 shows the optimized values of τ_h and τ_v during the mid and late season. The τ_v increased monotonically from 0.03 to 0.3, implying similar sensitivity of τ_v to crop growth during the mid and late season. It results in b_v values that are relatively stable between 0.04 and 0.048,

Table 3
RMSD and Bias, both in m^3/m^3, in retrieved SM estimates after DOY 180 in comparison with the *in situ* SM observed during at the corn site during SMAPVEX16-MicroWEX. N is the total number of T_B observations.

Optimization	VWC source	Overall (N = 6181)		VWC< 4 kg/m^2 (N = 1797)		VWC> 4 kg/m^2 (N = 4383)	
quantity		RMSD	bias	RMSD	bias	RMSD	bias
$T_{B,\,h}$	*in situ* VWC	0.023	0.005	0.023	0.005	0.022	0.008
	NDVI	0.029	−0.013	0.023	0.005	0.030	−0.020
	NDWI	0.024	0.005	0.029	0.013	0.022	0.002
	RVI	0.028	0.016	0.038	0.025	0.023	0.013
	CR_{vv}	0.024	0.009	0.029	0.014	0.022	0.008
	CR_{hh}	0.032	0.018	0.045	0.032	0.025	0.013
$T_{B,\,v}$	*in situ* VWC	0.028	−0.003	0.028	−0.013	0.028	−0.004
	NDVI	0.042	−0.030	0.032	−0.012	0.046	−0.035
	NDWI	0.031	−0.013	0.029	−0.008	0.032	−0.015
	RVI	0.060	−0.031	0.029	−0.005	0.067	−0.040
	CR_{vv}	0.028	−0.007	0.028	−0.008	0.029	−0.007
	CR_{hh}	0.065	−0.043	0.030	−0.007	0.073	−0.055

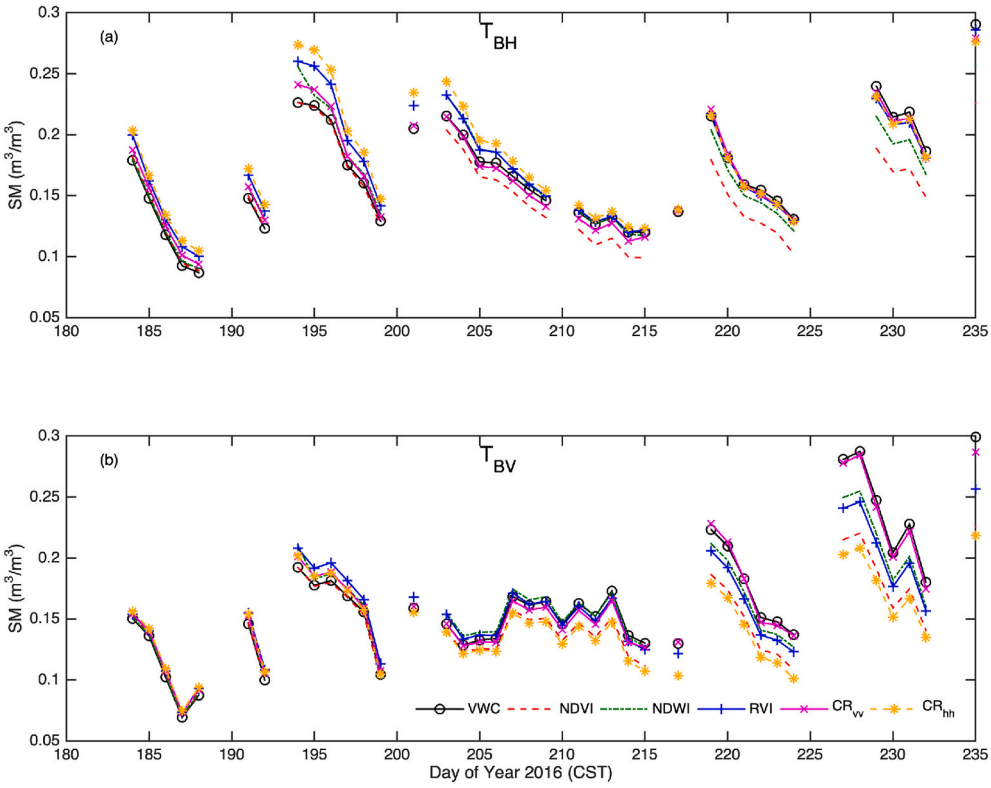

Fig. 12. Impact of different formulations of VWC on retrieved SM for corn. Retrieved SM from optimization of (a) H- and (b) V-pol brightness temperatures, with *in situ* VWC and VWCs derived from NDVI, NDWI, RVI, and CR relationships in Table 2. The black line is the retrieval using *in situ* VWC.

particularly once corn reaches 5 kg/m^2 (DOY 200). On the other hand, τ_h increased from 0.06 to about 0.3 till DOY 220 when VWC is 5.9 kg/m^2, after which it was stable. The resulting b_h values follow similar trend as the b_v values till DOY 205, after which they increase from 0.04 to about 0.05. Both b values at V- and H-pol for corn are lower than the values of 0.1–0.26, typically reported in literature (Dugwon et al., 2010). However, Wigneron et al. (2007) found b value lower than 0.1 for corn and more recently, Togliatti et al. (2019) reported similar values in Iowa.

4.4. *VWC from optical and radar indices and impact on SM retrievals*

Table 2 shows the regression equations for the VWC of corn obtained using optical and microwave indices, and their related statistics compared with the *in situ* VWC. The NDVI-derived VWC from the relationship used in the SMAP algorithm (6), had a higher RMSD and bias during the growing season. Both optical indices saturate when VWC is around 4 kg/m^2, since they measure surface reflectances, as seen in the time series regression in Figs. 10(a) and (b). Although the NDWI provides a lower Pearson correlation coefficient (R) value than the NDVI-derived VWC during the overall growing season, when comparing the two optical indices, it shows better performance during the vegetative stage when VWC $\leq$ 4 kg/m^2, with low bias and RMSD of 0.16 kg/m^2 and 0.21 kg/m^2, respectively. The *p*-value for the NDWI-VWC relationship was high at 0.07 for VWC $>$ 4 kg/m^2, indicating that a strong relationship between NDWI and VWC is unlikely in mid-late season. Cosh et al. (2019) found an RMSD of 1.37 kg/m^2 for their regression for VWC $<$ 4 kg/m^2 including 5 corn sites in the SMAP pixel. When their regression coefficients were applied to the SMAPVEX16-MicroWEX site, it resulted in similar results, as shown in Fig. 10, with an R of 0.93 and RMSD of 0.27 kg/m^2, indicating that the regression coefficients from SMAPVEX16-MicroWEX site were representative to the study region.

The regressions with microwave indices were conducted at an incidence angle of 50, based upon available *in situ* radar observations. In contrast with the optical indices, the microwave indices, RVI and CR_{vv} saturate at higher VWC values of 4–6 kg/m^2 (see Figs. 11(a) and (b)), since microwave signals penetrate the top layers of canopy and sense changes within the canopy and upper soil layers. Even though both RVI and CR_{vv} regressions had similar R values in Table 2, the bias, RMSD, and p-value for RVI were much higher than those for CR_{vv}, indicating that CR_{vv} is a better radar index for VWC estimation. In this study, the CR_{vv} values at L-band were $\leq$ 0.18 for VWC $\leq$ 6.4 kg/m^2. Vreugdenhil et al. (2018) found C-band CR_{vv} values ranging from 0.18 to 0.42 for VWC $\leq$ 7 kg/m^2 in their study. CR_{hh}-derived VWC had the highest RMSD, bias, and p-value, and the lowest R among all indices.

The index-VWC relationship is linear for both optical and microwave indices during low VWC, but becomes non-linear for microwave indices for high VWC values. For example, the RVI-VWC was non-linear when VWC $>$ 4 kg/m^2, while the CR_{vv}-VWC became non-linear when VWC $>$ 5 kg/m^2. The VWC estimated from NDVI using the relationship in eq. (6) is higher than the *in situ* VWC in the early season, but is lower in the late season. NDWI provides realistic VWC estimates till DOY 210, after which they are underestimated compared to the *in situ* VWC. Fig. 11(b) shows that the VWC estimated from CR_{vv} does a remarkable job of tracking the variations in *in-situ* VWC up to 6 kg/m^2. Thus, the NDWI and CR_{vv} together provide realistic VWC information over larger VWC ranges during the growing season.

Table 3 shows the RMSDs and bias of SM retrieved from H and V-pol T_B starting at DOY 180 onward compared with the *in situ* SM. The VWC was obtained from *in situ* observations and the five indices (Table 2). The NDWI- and CR_{vv}-derived VWCs provide the best retrievals, with the lowest seasonal RMSDs and biases, similar to their VWC comparisons in Table 2 and Figs. 10 and 11. In general, the RMSDs of retrieved SM were higher for V-pol T_B than for H-pol, particularly later in the season, as seen in Table 3 and Figs. 12(a) and (b). The SM using H-pol T_B had similar overall RMSDs and biases for all VWC formulations, while the retrievals using V-pol T_B had lower RMSDs and biases for NDWI- and CR_{vv}-derived VWC. Overall, VWC from all indices provided similar SM to that using *in situ* VWC until ear formation, when the *in situ* VWC was

close to 4 kg/m^2 (see Fig. 4(a)) and contribution from soil is still significant. As the canopy grows and the polarization-dependent corn structure plays increasingly dominant role after *in situ* VWC > 4 kg/m^2, higher RMSDs are observed with NDVI, RVI, and CR_{hh} (see Table 3), particularly for V-pol T_B. Since SM retrieval using *in situ* VWC is expected to perform the best and can be used as a reference dataset, as also seen in Table 3, the retrievals with index-derived VWCs are compared to the retrievals using *in situ* VWC in Figs. 12(a) and (b). Between the two optical indices, the NDVI provided consistently lower SM after DOY 200, when *in situ* VWC was about 4 kg/m^2. Among the radar indices, the CR_{vv} provided consistently better SM than RVI or CR_{hh} when compared to the retrieved SM using the *in situ* VWC. Thus, VWC derived from NDWI or L-band CR_{vv}, such as those from NISAR and ROSE-L, may provide the most consistent and realistic SM retrievals during the growing season.

5. Conclusions

This study provided insights into the differences and the seasonal trend of satellite- and field-scale passive signatures and retrieved soil moisture in agricultural regions, and investigated the impact of VWC information on SM retrievals at field-scale. It used high temporal resolution active and passive observations at L-band from the SMAPVEX16-MicroWEX. The ground-based passive observations matched well with those from SMAP at 36 km during the entire growing season, with SMAP T_B values lower than ground-based T_B for corn, but higher than the soybean T_B. The differences between the ground and SMAP T_Bs were further reduced when the ground-based T_Bs were upscaled to satellite footprint. However, despite the agreement in terms of T_Bs, the RMSD between the retrieved soil moisture from SMAP and upscaled SM was high at 0.05 m^3/m^3. This suggests that sub-footprint heterogeneity and VWC may be impacting SM retrievals during the growing season.

To investigate the impact of VWC on SM retrievals, a field-scale SCA SMAP retrieval algorithm was implemented using ground-based T_B at both polarizations along with VWC values obtained from optical and microwave indices. Overall, the NDWI- and CR_{vv} derived indices provided the lowest RMSDs and biases. While their performances were similar, the availability of microwaves during cloudy conditions is advantageous. The coefficients from this study may be used for similar corn cultivars and regions, such as the corn-belt in the United States. However, since the coefficients are vegetation-dependent, further studies are suggested for other crops. In addition, studies are also needed for high biomass crops since the RVI- and CR_{vv}-derived VWC indicated a need for higher-order relationships for VWC > 4–5 kg/m^2, and there are no deterministic VWC-levels for radar due to lack of studies in high biomass crops. The relationships may also be different for indices at other incidence angles and frequencies.

The results of this study are particularly relevant to SMAP SM retrieval in agricultural areas since the performance of the current SMAP baseline algorithm, SCA, is constrained by the degree to which the VWC data capture spatial and temporal variability during the growing season in these areas. Furthermore, the retrieval of SM from microwave observations is increasingly performed by combining data from multiple missions (*e.g.* SMAP and Sentinel-1 and/or Sentinel-2). This trend is likely to continue with the advent of new sensors such as NISAR, ROSE-L and CIMR. In these merged retrievals, optical and/or radar data are essential to account for heterogeneity impacts, particularly vegetation cover, when used with comparatively coarse passive data. The analysis and conclusions of this study are therefore relevant for microwave remote sensing of soil moisture in general.

Declaration of Competing Interest

The authors declare that they have no known competing financial interests or personal relationships that could have appeared to influence the work reported in this paper.

Acknowledgments

The authors thank anonymous reviewers for their helpful comments and suggestions. The SMAPVEX16-MicroWEX was funded by grant from the NASA-Terrestrial Hydrology Program (award number: NNX16AQ24G). The work of S. C. Steele-Dunne was supported by a Vidi Grant 14126 from the Dutch Technology Foundation TTW, which is part of the Netherlands Organization for Scientific Research (NWO), and partly funded by the Ministry of Economic Affairs. The work of A. Monsivais-Huertero was supported by the National Council of Science and Technology of Mexico (project AEM-2014-1-247741). In addition to the financial support from various agencies above, the SMAPVEX16-MicroWEX team is thankful to David and Annette Sweeney; John Prueger, Forrest Goodman, and Jerry Hatfield from USDA-ARS; and Prof. Brian Hornbuckle and his research team at Iowa State University for providing field support during the field campaign.

References

Bhuiyan, H., McNairn, H., Powers, J., Friesen, M., Pacheco, A., Jackson, T.J., Cosh, M., Colliander, A., Berg, A., Rowlandson, T., Bullock, P., Magagi, R., 2018. Assessing SMAP soil moisture scaling and retrieval in the Carman study site. Vadose Zone J. 17, 1–14. https://doi.org/10.2136/vzj2018.07.0132.

Bongiovanni, T., Liu, P., Nagarajan, K., Preston, D., Rush, P., Duan, X., Chen, G., Terwilleger, R., Monsivais-Huertero, A., Judge, J., De Roo, R., Akbar, R., Morris, M., Williams, O., Marks, L., Cardozo, C., Moghaddam, M., England, A., 2015a. Field observations during the tenth microwave water and energy balance experiment (MicroWEX-10): from March 1, 2011 through January 5, 2012. In: Technical report. Center for Remote Sensing, University of Florida http://edis.ifas.ufl.edu/ae512.

Bongiovanni, T., Liu, P., Nagarajan, K., Preston, D., Rush, P., van Emmerik, T., Terwilleger, R., Monsivais-Huertero, A., Judge, J., Steele-Dunne, S., De Roo, R., Akbar, R., Baar, E., Wallace, M., England, A., 2015b. Field observations during the eleventh microwave water and energy balance experiment (MicroWEX-11): from April 25, 2012 through December, 2012. In: Technical report. Center for Remote Sensing, University of Florida http://edis.ifas.ufl.edu/ae514.

Casanova, J.J., Judge, J., Jones, J.W., 2006. Calibration of the ceres-maize model for linkage with a microwave remote sensing model. Trans. ASAE 49, 783–792. https://doi.org/10.13031/2013.20036.

Chan, S., Bindlish, R., O'Neill, P., Njoku, E., Jackson, T., Colliander, A., Chen, F., Burgin, M., Dunbar, S., Piepmeier, J., Yueh, S., Entekhabi, D., Cosh, M., Caldwell, T., Walker, J., Wu, X., Berg, A., Rowlandson, T., Pacheco, A., McNairn, H., Thibeault, M., Martínez-Fernández, J., González-Zamora, A., Seyfried, M., Bosch, D., Starks, P., Goodrich, D., Prueger, J., Palecki, M., Small, E., Zreda, M., Calvet, J., Crow, W., Kerr, Y., 2016. Assessment of the SMAP passive soil moisture product. *IEEE trans. Geosci.* Remote Sens. 54, 4994–5007. https://doi.org/10.1109/TGRS.2016.2561938.

Chen, D., Huang, J., Jackson, T., 2005. Vegetation water content estimation for corn and soybeans using spectral indices derived from MODIS near- and short-wave infrared bands. Remote Sens. Environ. 98, 225–236. https://doi.org/10.1016/j.rse.2005.07.008.

Choudhury, B., Schmugge, T.J., Chang, A., Newton, R., 1979. Effect of surface roughness on the microwave emission from soils. J. Geophys. Res. 84, 5699–5706.

Claassen, M., Shaw, R., 1970. Water deficit effects on corn. II. Grain components. Agron. J. 62, 652–655. https://doi.org/10.2134/agronj1970.00021962006200050032x.

Clevers, J., Zurita-Milla, R., 2008. 3 - multisensor and multiresolution image fusion using the linear mixing model. In: Stathaki, T. (Ed.), Image Fusion. Academic Press, Oxford, pp. 67–84. https://doi.org/10.1016/B978-0-12-372529-5.00004-4.

Colliander, A., Jackson, T., McNairn, H., Chazanoff, S., Dinardo, S., Latham, B., O'Dwyer, I., Chun, W., Yueh, S., Njoku, E., 2015. Comparison of airborne passive and active L-band system (PALS) brightness temperature measurements to SMOS observations during the SMAP validation experiment 2012 (SMAPVEX12). IEEE Geosc. Rem. Sens. Letters 12, 801–805.

Colliander, A., Cosh, M., Misra, S., Jackson, T., Crow, W., Chan, S., Bindlish, R., Chae, C., Collins, C., Yueh, S., 2017a. Validation and scaling of soil moisture in a semi-arid environment: SMAP validation experiment 2015 (SMAPVEX15). Remote Sens. Environ. 196, 101–112. https://doi.org/10.1016/j.rse.2017.04.022.

Colliander, A., Jackson, T., Bindlish, R., Chan, S., Das, N., Kim, S., Cosh, M., Dunbar, R., Dang, L., Pashaian, L., Asanuma, J., Aida, K., Berg, A., Rowlandson, T., Bosch, D., Caldwell, T., Caylor, K., Goodrich, D., Jassar, H., Lopez-Baeza, E., Martínez-Fernández, J., González-Zamora, A., Livingston, S., McNairn, H., Pacheco, A., Moghaddam, M., Montzka, C., Notarnicola, C., Niedrist, G., Pellarin, T., Prueger, J., Pulliainen, J., Rautiainen, K., Ramos, J., Seyfried, M., Starks, P., Su, Z., Zeng, Y., van der Velde, R., Thibeault, M., Dorigo, W., Vreugdenhil, M., Walker, J., Wu, X., Monerris, A., O'Neill, P., Entekhabi, D., Njoku, E., Yueh, S., 2017b. Validation of SMAP surface soil moisture products with core validation sites. Remote Sens. Environ. 191, 215–231. https://doi.org/10.1016/j.rse.2017.01.021.

Colliander, A., Cosh, M., Misra, S., Jackson, T., Crow, W., Powers, J., McNairn, H., Bullock, P., Berg, A., Magagi, R., Gao, Y., Bindlish, R., Williamson, R., Ramos, I., Latham, B., O'Neill, P., Yueh, S., 2019. Comparison of high-resolution airborne soil moisture retrievals to SMAP soil moisture during the SMAP validation experiment

2016 (SMAPVEX16). Remote Sens. Environ. 227, 137–150. https://doi.org/10.1016/j.rse.2019.04.004.
Coopersmith, E., Cosh, M., Petersen, W., Prueger, J., Niemeier, J., 2015. Soil moisture model calibration and validation: an ARS watershed on the south fork Iowa River. J. Hydrometeorol. 16, 1087–1101. https://doi.org/10.1175/JHM-D-14-0145.1.
Cosh, M., Tao, J., Jackson, T., McKee, L., O'Neill, P., 2010. Vegetation water content mapping in a diverse agricultural landscape: National Airborne Field Experiment 2006. J. Applied Rem. Sensing 4, 043532. https://doi.org/10.1117/1.3449090.
Cosh, M., White, W., Colliander, A., Jackson, T., Prueger, J., Hornbuckle, B., Hunt, E., McNairn, H., Powers, J., Walker, V., Bullock, P., 2019. Estimating vegetation water content during the soil moisture active passive validation experiment 2016. J. Applied Rem. Sensing 13, 014516. https://doi.org/10.1117/1.JRS.13.014516.
Denmead, O., Shaw, R., 1960. The effects of soil moisture stress at different stages of growth on the development and yield of corn. Agron. J. 52, 272–274. https://doi.org/10.2134/agronj1960.00021962005200050010x.
Dingman, S., 2015. Physical Hydrology. Waveland Press, Inc., Illinois, USA.
Donlon, C., 2019. Copernicus Imaging Microwave Radiometer (CIMR) Mission Requirements Document. Technical Report https://cimr.eu/.
Dugwon, S., Lakhankar, T., Khanbilvardi, R., 2010. Sensitivity analysis of b-factor in microwave emission model for soil moisture retrieval: A case study for SMAP mission. Remote Sens. 2, 1273–1286. https://doi.org/10.3390/rs2051273.
Entekhabi, D., Njoku, E.G., O'Neill, P.E., Kellogg, K.H., Crow, W.T., Edelstein, W.N., Entin, J.K., Goodman, S.D., Jackson, T.J., Johnson, J., Kimball, J., Piepmeier, J.R., Koster, R.D., Martin, N., McDonald, K.C., Moghaddam, M., Moran, S., Reichle, R., Shi, J.C., Spencer, M.W., Thurman, S.W., Tsang, L., Van Zyl, J., 2010. The soil moisture active passive (SMAP) mission. Proc. IEEE 98, 704–716.
Fan, X., Liu, Y., Gan, G., Wu, G., 2020. SMAP underestimates soil moisture in vegetation-disturbed areas primarily as a result of biased surface temperature data. Remote Sens. Environ. 247, 111914.
Gao, Y., Walker, J., Allahmoradi, M., Monerris, A., Ryu, D., Jackson, T.J., 2015. Optical sensing of vegetation water content: A systhesis study. IEEE J. Selected Topics in Appplied Earth Obs. and Rem. Sens. 8, 1456–1464. https://doi.org/10.1109/JSTARS.2015.2398034.
Hoekman, D., 1991. Speckle ensemble statistics of logarithmically scaled data. *IEEE trans. Geosci.* Remote Sens. 29, 180–182. https://doi.org/10.1109/36.103311.
Huang, Y., Walker, J., Gao, Y., Wu, X., Monerris, A., 2015. Estimation of vegetation water content from the radar vegetation index at L-band. *IEEE trans. Geosci.* Remote Sens. 54, 981–989. https://doi.org/10.1109/TGRS.2015.2471803.
Hunt, E., Li, L., Yilmaz, M., Jackson, T., 2011. Comparison of vegetation water contents derived from shortwave-infrared and passive-microwave sensors over Central Iowa. Remote Sens. Environ. 115, 2376–2383. https://doi.org/10.1016/j.rse.2011.04.037.
Jackson, T., Chen, D., Cosh, M., Li, F., Anderson, M., Walthall, C., Doriaswamy, P., Hunt, E., 2004. Vegetation water content mapping using Landsat data derived normalized difference water index for corn and soybeans. Remote Sens. Environ. 92, 475–482. https://doi.org/10.1016/j.rse.2003.10.021.
Kankaku, Y., Suzuki, S., Shimada, M., 2015. ALOS-2 first year operation result. In: IEEE Int. Geosc. And rem. Sens. Symposium, Proc. IGARSS, 2015, pp. 4121–4124. https://doi.org/10.1109/IGARSS.2015.7326732.
Kankaku, Y., Suzuki, S., Motohka, T., Ohki, M., Natsuaki, R., Shimada, M., 2016. ALOS-2 operation status. In: IEEE Int. Geosc. And rem. Sens. Symposium, Proc. IGARSS, 2016, pp. 3846–3848. https://doi.org/10.1109/IGARSS.2016.7729997.
Kerr, Y., Waldteufel, P., Wigneron, J., Martinuzzi, J., Font, J., Berger, M., 2001. Soil moisture retrieval from space: the soil moisture and ocean salinity (SMOS) mission. IEEE Trans. Geosci. Remote Sens. 39, 1729–1735. https://doi.org/10.1109/36.942551.
Kim, Y., Jackson, T., Bindlish, R., Lee, H., Hong, S., 2012. Radar vegetation index for estimating the vegetation water content of rice and soybean. IEEE Geosc. Rem. Sens. Letters 9, 564–568. https://doi.org/10.1109/LGRS.2011.2174772.
Kim, Y., Jackson, T., Bindlish, R., Hong, S., Jung, G., Lee, K., 2014. Retrieval of wheat growth parameters with radar vegetation indices. IEEE Geosc. Rem. Sens. Letters 11, 808–812. https://doi.org/10.1109/LGRS.2013.2279255.
Konings, A.G., Yu, Y., Xu, L., Yang, Y., Schimel, D., Saatchi, S., 2017. Active microwave observations of diurnal and season variations of canopy water content in humid african tropical forests. Geophys. Res. Lett. 44, 2290–2299. https://doi.org/10.1002/2016GL072388.
Lawrenmce, H., Wigneron, J., Demontoux, F., Mialon, A., Kerr, Y., 2013. Evaluating the semiempirical H-Q model used to calculate the L-band emissivity of a rough bare soil. IEEE Trans. Geosci. Remote Sens. 51, 4075–4084. https://doi.org/10.1109/TGRS.2012.2226995.
Li, X., Al-Yaari, A., Schwank, M., Fan, L., Frappart, F., Swenson, J., Wigneron, J., 2020. Compared performances of SMOS-IC soil moisture and vegetation optical depth retrievals based on tau-omega and two-stream microwave emission models. Remote Sens. Environ. 236. https://doi.org/10.1016/j.rse.2019.111502.
Liu, P., De Roo, R., England, A., Judge, J., 2013. Impact of moisture distribution within the sensing depth of L- and C-band emission of sandy soils. IEEE J. Selected Topics in Appplied Earth Obs. and Rem. Sens. 6, 887–899. https://doi.org/10.1109/JSTARS.2012.2213239.
Liu, P., Judge, J., De Roo, R., England, A., Bongiovanni, T., 2016a. Uncertainty in soill moisture retrievals using the SMAP combined active-passive algorithm for growing sweet corn. IEEE J. Selected Topics in Appplied Earth Obs. and Rem. Sens. 9, 3326–3339. https://doi.org/10.1109/JSTARS.2016.2562660.
Liu, P., Judge, J., De Roo, R., England, A., Bongiovanni, T., Luke, A., 2016b. Dominant backscattering mechanisms at L-band during dynamic soil moisture conditions for sandy soils. Remote Sens. Environ. 178, 104–112. https://doi.org/10.1016/j.rse.2016.02.062.
McNairn, H., Brisco, B., 2004. The application of C-band polarimetric SAR for agriculture: a review. *Can. J.* Remote Sens. 30, 525–542. https://doi.org/10.5589/m03-069.
McNairn, H., Jackson, T., Wiseman, G., Bélair, S., Berg, A., Bullock, P., Colliander, A., Cosh, M., Kim, S., Magagi, R., Moghaddam, M., Njoku, E., Adams, J., Homayouni, S., RoTimi Ojo, E., Rowlandson, T., Shang, J., Goïta, K., Hosseini, M., 2015. The soil moisture active passive validation experiment 2012 (SMAPVEX12): prelaunch calibration and validation of the SMAP soil moisture algorithms. *IEEE trans. Geosci.* Remote Sens. 53, 2784–2801.
Mialon, A., Wigneron, J., deRosnay, P., Escorihuela, M.J., Kerr, Y., 2012. Evaluating the L-MEB model from long-term microwave measurements over a rough field, SMOSREX 2006. IEEE Trans. Geosci. Remote Sens. 50, 1458–1467. https://doi.org/10.1109/TGRS.2011.2178421.
Mironov, V., Kosolapova, L., Fomin, S., 2009. Physically and mineralogically based spectroscopic dielectric model for moist soils. IEEE Trans. Geosci. Remote Sens. 47, 2059–2070. https://doi.org/10.1109/TGRS.2008.2011631.
Monsivais-Huertero, A., Judge, J., 2011. Comparison of bacscattering models at L-band for growing corn. IEEE Geosc. Rem. Sens. Letters 8, 24–28. https://doi.org/10.1109/LGRS.2010.2050459.
Monsivais-Huertero, A., Graham, W., Judge, J., Agrawal, D., 2010. Effect of simultaneous state–parameter estimation and forcing uncertainties on root-zone soil moisture for dynamic vegetation using EnKF. Adv. Water Resour. 33, 468–484. https://doi.org/10.1016/j.advwatres.2010.01.011.
Monsivais-Huertero, A., Liu, P., Judge, J., 2018. Phenology-based backscattering model for corn at L-band. IEEE Trans. Geosci. Remote Sens. 56, 4989–5005.
Motohka, T., Kankaky, Y., Suzuki, S., 2017. Advanced Land observing Satellite-2 (ALOS-2) and its follow-on L-band SAR mission. In: IEEE radar conference, Proc. IEEE RadarConf, 2017, pp. 953–956. https://doi.org/10.1109/RADAR.2017.7944341.
Nagarajan, K., Judge, J., 2013. Spatial scaling and variability of soil moisture over heterogeneous land cover and dynamic vegetation conditions. IEEE Geosc. Rem. Sens. Letters 10, 880–884. https://doi.org/10.1109/LGRS.2012.2226430.
Nagarajan, K., Liu, P., DeRoo, R., Judge, J., Akbar, R., Rush, P., Feagle, S., Preston, D., Terwilleger, R., 2014. Automated L-band radar system for sensing soil moisture at high temporal resolution. IEEE Geosc. Rem. Sens. Letters 11, 504–508. https://doi.org/10.1109/LGRS.2013.2270453.
O'Neill, P., Joseph, A., Srivastava, P., Cosh, M., Lang, R., 2014. Seasonal parameterizations of the tau-omega model using the ComRAD ground-based SMAP simulator. In: IEEE Int. Geosc. And rem. Sens. Symposium, Proc. IGARSS, 2014, pp. 2423–2426. https://doi.org/10.1109/IGARSS.2014.6946961.
O'Neill, P., Chan, S., Njoku, E., Jackson, T., Bindlish, R., 2018. Algorithm theoretical basis document level 2 and 3 soil moisture (passive) data products, version D. June 6, 2018. JPL D-66480. In: Technical report. Jet Propulsion Laboratory, California Institute of Technology. Pasadena, CA, USA.
Pierdicca, N., Davidson, M., Chini, M., Dierking, W., Djavidnia, S., Haarpaintner, J., Hajduch, G., Laurin, G., Lavalle, M., Lopez-Martinex, C., Nagler, T., Su, B., 2019. The copernicus L-band SAR mission ROSE-L (Radar Observing System for Europe) (Conference Presentation). In: Bovenga, F., Notarnicola, C., Pierdicca, N., Santi, E. (Eds.), Active and passive microwave remote sensing for environmental monitoring III, International Society for Optics and Photonics. SPIE, pp. 1–180. https://doi.org/10.1117/12.2534743.
Prakash, R., Singh, D., Pathak, N.P., 2012. A fusion approach to retrieve soil moisture with Sar and optical data. IEEE J. Selected Topics in Appplied Earth Obs. and Rem. Sens. 5, 36–56. https://doi.org/10.1109/JSTARS.2011.2169236.
Roberto, C., Lorenzo, B., Michele, M., Michol, R., Cinzia, P., 2016. In: Thenkabail, P., Lyon, J., Huete, A. (Eds.), Optical remote sensing of vegetation water content. Hyperspectral remote sensing of vegetation. CRC press, p. 227.
Rondinelli, W., Hornbuckle, B., Patton, J., Cosh, M., Walker, V., Carr, B., Logsdon, S., 2015. Different rates of soil drying after rainfall are observed by the SMOS satellite and the south fork in situ soil moisture network. J. Hydrometeorol. 16, 889–903. https://doi.org/10.1175/JHM-D-14-0137.1.
Rosen, P., Hensley, S., Shaffer, S., Veilleux, L., Chakraborty, M., Misra, T., Bhan, R., Sagi, V., Satish, R., 2015. The NASA-ISRO SAR mission - an international space partnership for science and societal benefit. In: Radar Conference (RadarCon), 2015 IEEE, pp. 1610–1613. https://doi.org/10.1109/RADAR.2015.7131255.
Rosen, P., Hensley, S., Shaffer, S., Edelstein, W., Kim, Y., Kumar, R., Misra, T., Bhan, R., Satish, R., Sagi, R., 2016. An update on the NASA-ISRO dual-frequency DBF SAR (NISAR) mission. In: IEEE Int. Geosc. And rem. Sens. Symposium, Proc. IGARSS, 2016, pp. 2106–2108. https://doi.org/10.1109/IGARSS.2016.7729543.
Rosen, P., Hensley, S., Shaffer, S., Edelstein, W., Kim, Y., Kumar, R., Misra, T., Bhan, R., Sagi, R., 2017. The NASA-ISRO SAR (NISAR) mission dual-band radar instrument preliminary design. In: IEEE Int. Geosc. And rem. Sens. Symposium, Proc. IGARSS, 2017, pp. 3832–3835. https://doi.org/10.1109/IGARSS.2017.8127836.
Sharma, A., Land, R., Kurum, M., O'Neill, P., Cosh, M.H., 2020. L-band radar experiment and modeling of corn canopy over a full growing season. *IEEE trans. Geosci.* Remote Sens. 58, 5821–5835.
Steele-Dunne, S., Friesen, J., van de Giesen, N., 2012. Using diurnal variation in backscatter to detect vegetation water stress. IEEE Trans. Geosci. Remote Sens. 5, 2618–2629. https://doi.org/10.1109/TGRS.2012.2194156.
Steele-Dunne, S., McNairn, H., Monsivais-Huertero, A., Judge, J., Liu, P., Papathanassiou, K., 2017. Radar remote sensing of agricultural canopies: A review. IEEE Trans. Geosci. Remote Sens. 10, 2249–2273. https://doi.org/10.1109/JSTARS.2016.2639043.
Stiles, J.M., Sarabandi, K., Ulaby, F., 2000. Electromagnetic scattering from grassland. II. Measurement and modeling results. IEEE Trans. Geosci. Remote Sens. 38, 349–356.
Tavakoli, A., Sarabandi, K., Ulaby, F., 1991. Horizontal propagation through periodic vegetation canopies. IEEE Trans. Ant. Prop. 39, 1014–1023.

Tien, K., De Roo, R., Judge, J., Pham, H., 2007. Comparison of calibration techniques for ground-based C-band radiometers. IEEE Geosc. Rem. Sens. Letters 4, 83–87. https://doi.org/10.1109/LGRS.2006.886420.

Togliatti, K., Hartman, T., Walker, V., Arkebauer, T.J., Suyker, A., VanLoocke, A., Hornbuckle, B., 2019. Satellite L-band vegetation optical depth is directly proportional to crop water in the US corn belt. Remote Sens. Environ. 233, 111378. https://doi.org/10.1016/j.rse.2019.111378.

Ulaby, F., Elachi, C., 1990. Radar Polarimetry for Geoscience Applications. Artech House, Norwood, MA.

Ulaby, F., Long, D., Blackwell, W., Elachi, C., Fung, A., Ruf, C., Sarabandi, K., Zebker, H., Van Zyl, J., 2014. Microwave Radar and Radiometric Remote Sensing. University of Michigan Press.

USDA, 2016. National Agricultural Statistics Service Cropland Data Layer. URL. https://nassgeodta.gmu.edu/CropScape/.

Van de, A., Wigneron, J.P., 2004. The b-factor as a function of frequency and canopy type at H-polarization. IEEE Trans. Geosci. Remote Sens. 42, 786–794. https://doi.org/10.1109/TGRS.2003.821889.

van Emmerik, T., Steele-Dunne, S., Paget, A., Oliveira, R., Bittencourt, P.L., Barros, F.D. V., van de Giesen, N., 2017. Water stress detection in amazon using radar. Geophys. Res. Lett. 44, 6841–6849. https://doi.org/10.1002/2017GL073747.

Vermunt, P., Khabbazan, S., Steele-Dunne, S., Judge, J., Monsivais-Huertero, A., Guerriero, L., Liu, P., 2020. Response of subdaily L-band backscatter to internal and surface canopy water dynamics. IEEE Trans. Geosci. Remote Sensing 1–16. https://doi.org/10.1109/TGRS.2020.3035881.

Vreugdenhil, M., Wagner, W., Bauer-Marschallinger, B., Pfeil, I., Teubner, I., Rüdiger, C., Strauss, P., 2018. Sensitivity of Sentinel-1 backscatter to vegetation dynamics: an Austrian case study. Remote Sens. 10, 1396. https://doi.org/10.3390/rs10091396.

Walker, V., Hornbuckle, B., Cosh, M., Prueger, J., 2019. Seasonal evaluation of SMAP soil moisture in the US corn belt. Remote Sens. 11 https://doi.org/10.3390/rs11212488.

Wang, J.R., Choudhury, B.J., 1981. Remote sensing of soil moisture content over bare field at 1.4 GHz frequency. J. Geophys. Res. 86, 5277–5282. https://doi.org/10.1029/JC086iC06p05277.

Wigneron, J., Kerr, Y., Waldteufel, Y., Saleh, K., Escorihuela, M.J., Richaume, P., Ferrazoli, P., de Rosnay, P., Gurney, R., Calvet, J.C., Grant, J., Guglielmetti, M., Hornuckle, B., Matzler, C., Pellarin, T., Schwank, M., 2007. L-band microwave emission of the biosphere (L-ME) model: description and claibration against experimental datasets over crop fields. Remote Sens. Environ. 107, 639–655. https://doi.org/10.1016/j.rse.2006.10.014.

Wigneron, J., Jackson, T.J., O'Neill, P., Lannoy, G.D., Rosnay, P.D., Walker, J.P., Ferrazzoli, P., Mironov, V., Bircher, S., Grant, J.P., Kurum, M., Schwank, M., Munoz-Sabater, J., Das, N., Royer, A., Al Biar, A.A.Y., Fernandez-Moran, R., Lawrence, H., Mialon, A., Parrens, M., Richaume, P., Delwart, S., Kerr, Y., 2017. Modelling the passive microwave signatures from land surfaces: A review of recent results and application to the L-band SMOS and SMAP soil moisture retrieval algorithms. Remote Sens. Environ. 192 https://doi.org/10.1016/j.rse.2017.01.024.

Yang, M., Calvin, K., Casanova, J., Judge, J., 2005. Measurements of soil surface roughness during the fourth microwave water and energy balance experiment: April 18 through June 13, 2005. In: Technical report. Center for Remote Sensing, University of Florida http://edis.ifas.ufl.edu/AE363.

Yilmaz, M., Hunt Jr., D., Goins, L., Ustin, S., Vanderbilt, V., Jackson, T., 2008. Vegetation water content during SMEX04 from ground data and Landsat 5 thematic mapper imagery. Remote Sens. Environ. 112, 350–362. https://doi.org/10.1016/j.rse.2007.03.029.

Zwieback, S., Colliander, A., Cosh, M.H., Martnez-Fernández, J., McNairn, H., Starks, P. J., Thibeault, M., Berg, A., 2018. Estimating time-dependent vegetation biases in the SMAP soil moisture product. Hydrol. Earth Syst. Sci. 22, 4473–4489.